





# HIV-1 Vpr Induces Degradation of Gelsolin, a Myeloid Cell-Specific Host Factor That Reduces Viral Infectivity by Inhibiting the Expression and Packaging of the HIV-1 Env Glycoprotein

Helena Fabryova,<sup>a</sup> Sandra Kao,<sup>a</sup> Sayaka Sukegawa,<sup>a\*</sup> Eri Miyagi,<sup>a</sup>  Louis Taylor,<sup>a</sup> § Damien Ferhadian,<sup>a</sup> Hideki Saito,<sup>a</sup>  Heiner Schaal,<sup>b</sup> Frank Hillebrand,<sup>b</sup>  Klaus Strebel<sup>a</sup>

<sup>a</sup>Laboratory of Molecular Microbiology, National Institute of Allergy and Infectious Diseases, NIH, Bethesda, Maryland, USA

<sup>b</sup>Institute of Virology, Medical Faculty, Heinrich Heine University Düsseldorf, Düsseldorf, Germany

**ABSTRACT** Gelsolin (GSN) is a structural actin-binding protein that is known to affect actin dynamics in the cell. Using mass spectrometry, we identified GSN as a novel Vpr-interacting protein. Endogenous GSN protein was expressed at detectable levels in monocyte-derived macrophages (MDM) and in THP-1 cells, but it was undetectable at the protein level in other cell lines tested. The HIV-1 infection of MDM was associated with a reduction in GSN steady-state levels, presumably due to the Vpr-induced degradation of GSN. Indeed, the coexpression of GSN and Viral protein R (Vpr) in transiently transfected HEK293T cells resulted in the Vpr-dependent proteasomal degradation of GSN. This effect was observed for Vprs from multiple virus isolates. The overexpression of GSN in HEK293T cells had no effect on Gag expression or particle release, but it reduced the expression and packaging of the HIV-1 envelope (Env) glycoprotein and reduced viral infectivity. An analysis of the HIV-1 splicing patterns did not reveal any GSN-dependent differences, suggesting that the effect of GSN on Env expression was regulated at a posttranscriptional level. Indeed, the treatment of transfected cells with lysosomal inhibitors reversed the effect of GSN on Env stability, suggesting that GSN reduced Env expression via enhanced lysosomal degradation. Our data identify GSN as a macrophage-specific host antiviral factor that reduces the expression of HIV-1 Env.

**IMPORTANCE** Despite dramatic progress in drug therapies, HIV-1 infection remains an incurable disease that affects millions of people worldwide. The virus establishes long-lasting reservoirs that are resistant to currently available drug treatments and allow the virus to rebound whenever drug therapy is interrupted. Macrophages are long-lived cells that are relatively insensitive to HIV-1-induced cytopathicity and thus could contribute to the viral reservoir. Here, we identified a novel host factor, gelsolin, that is expressed at high levels in macrophages and inhibits viral infectivity by modulating the expression of the HIV-1 Env glycoprotein, which is critical in the spread of an HIV-1 infection. Importantly, the viral protein Vpr induces the degradation of gelsolin and thus counteracts its antiviral activity. Our study provides significant and novel insights into HIV-1 virus-host interactions and furthers our understanding of the importance of Vpr in HIV-1 infection and pathogenesis.

**KEYWORDS** Vpr, gelsolin, human immunodeficiency virus, virus host interactions

Lentiviruses encode several accessory proteins, including Vif, Vpr, Vpu, Vpx, and Nef, that assist with virus replication at various steps of the replication cycle. While the functions of most of these accessory proteins is reasonably well-understood, the precise function of Vpr is still unclear. Vpr has been shown to induce the degradation of multiple cellular proteins, including the uracil-DNA glycosylases UNG2 and SMUG1 (1),

**Editor** Stephen P. Goff, Columbia University Medical Center

This is a work of the U.S. Government and is not subject to copyright protection in the United States. Foreign copyrights may apply.

Address correspondence to Klaus Strebel, [kstrebel@nih.gov](mailto:kstrebel@nih.gov).

\*Present address: Sayaka Sukegawa, Department of Molecular Virology, Tokyo Medical and Dental University, Tokyo, Japan.

§Present address: Louis Taylor, Department of Microbiology and Immunology, University of Maryland, Baltimore, Maryland, USA.

The authors declare no conflict of interest.

**Received** 25 October 2022

**Accepted** 7 December 2022

**Published** 5 January 2023

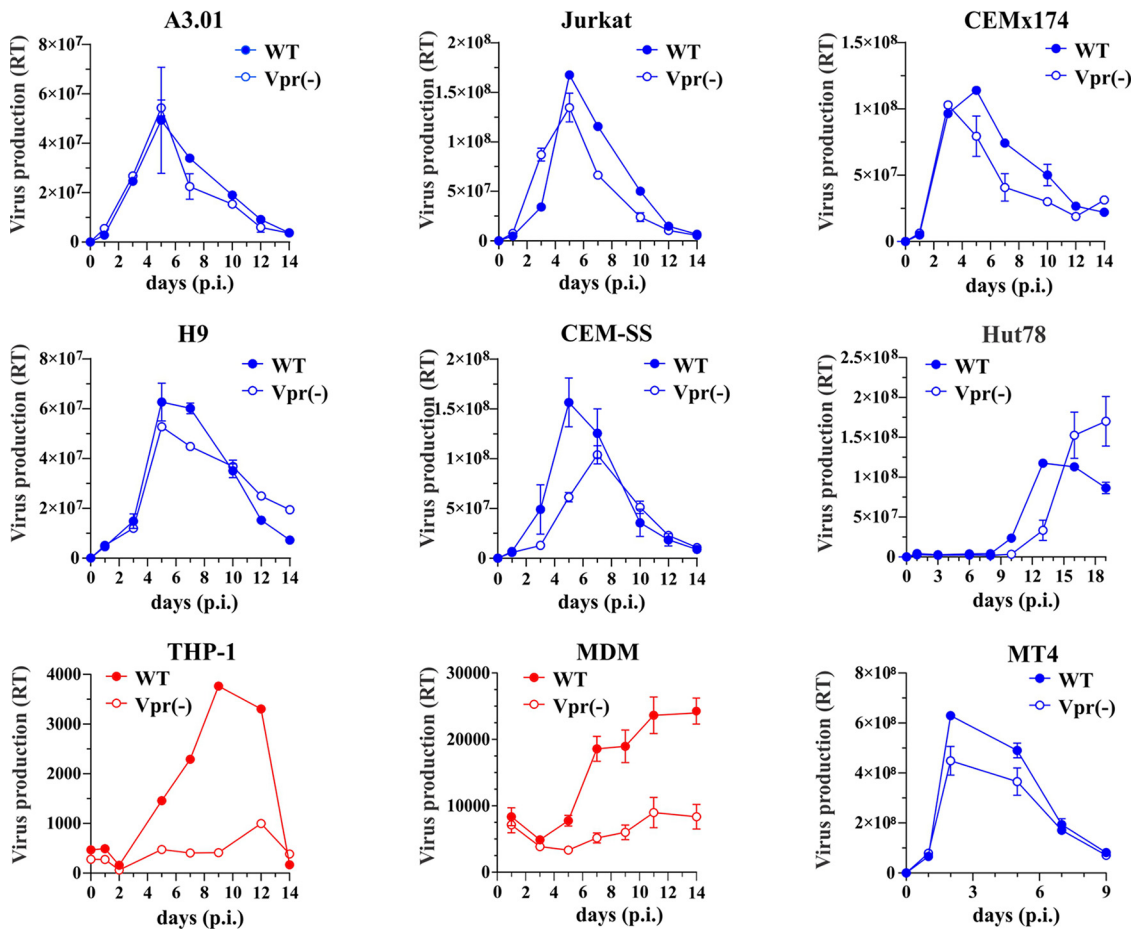


**FIG 1** The importance of Vpr in HIV-1 replication is cell-type dependent. Wild type or Vpr-defective NL4-3 (X4-tropic) and AD8 (R5-tropic) virus stocks were used to infect a variety of cell lines, as indicated. A3.01, Jurkat, CEMx174, H9, CEM-SS, Hut78, and MT4 cells were infected with equal RT units of X4-tropic wild type or Vpr (-) NL4-3 (graphed in blue), whereas THP-1 and MDM were infected with equal RT units of R5-tropic wild type or Vpr (-) AD8 virus (graphed in red). Virus replication was monitored by measuring the virus-associated RT activity (50), which was plotted as a function of time. The error bars reflect the standard error of the mean from triplicate infections.

IRF-3 (2), Zip (3), MCM10 (4), chromatin-associated Class I HDACs (5), CTIP2 (6), HLTF (7–9), Exo1 (10), and PCIF1 (11). The degradation of these proteins by Vpr is initiated by the recruitment of DCAF1/VprBP, a receptor of the Cul4-DDB1 ubiquitin ligase (1, 12–14), and it is followed by the assembly of an active E3 ubiquitin ligase complex that ultimately triggers the proteasomal degradation of Vpr binding partners. However, the importance of the Vpr-mediated degradation of these factors for virus replication in primary human cells remains largely unclear. Part of the problem with the functional analyses is that the deletion of Vpr does not cause significant virus restriction in most cell line models of HIV infection. Indeed, only monocytic cell types, such as THP-1 or MDM, consistently restricted the replication of Vpr-defective HIV-1 (Fig. 1), suggesting that these cells express sufficiently high levels of viral restriction factors so as to require neutralization by Vpr.

Since THP-1 cells can easily be grown in quantities that are large enough for proteomics studies, we performed a proteomic screen for Vpr-interacting proteins, using lysate from differentiated human THP-1 cells. One of the proteins identified in our screen was GSN. GSN is an 81 to 85 kDa actin-binding cellular protein that exists in two isoforms in humans (15, 16). Isoform 1 encodes an N-terminal signal peptide that allows the protein to be secreted, and it is therefore also referred to as plasma gelsolin. The cytoplasmic isoform 2 is derived from the differential splicing of the GSN mRNA and is initiated at an internal AUG codon; thus, it lacks 25 N-terminal residues, relative

to isoform 1 (15–18). Both isoforms are thought to exist in GSN-expressing cells, although their relative abundance is difficult to assess due to their similar electrophoretic mobilities. The physiological role of GSN is to regulate actin dynamics by modulating actin filament length in a  $\text{Ca}^{2+}$ -dependent manner (19). GSN is one of the most potent actin severing agents in the cell (20). Of note, GSN expression was found to be markedly reduced in breast cancers of humans, mice, and rats (21). GSN expression was also diminished in *H-ras* transformed mouse fibroblasts, human fibroblasts, and epithelial cells transformed by SV40 virus, gastric carcinoma cell lines, bladder cancer cell lines, and most bladder cancers (22–24). On the other hand, bacterial infections have been reported to increase GSN expression in macrophages (25), and GSN was found to inhibit Lipopolysaccharide (LPS)-induced inflammatory responses (26). Interestingly, GSN was upregulated in the brain tissue of SIV-infected macaques *in vivo*, whereas cytoplasmic GSN levels were shown to be reduced in HIV-infected macrophages (17). Finally, GSN was previously reported to be involved in Vpr-induced host cell apoptosis (27), and it was shown to be involved in the control of early HIV-1 infection through the restructuring of cortical F-actin (28). However, mechanistic details remain unclear.

The goals of our study were to better understand the role of GSN in HIV-1 replication and to characterize the functional interactions of GSN and Vpr. We observed the expression of GSN protein only in MDM, monocytic THP-1 cells, and PBMC. The expression of GSN was not Interferon (IFN) inducible. Instead, the coexpression of GSN and Vpr in transfected HEK293T or HeLa cells led to the inhibition of GSN expression. This adds GSN to the growing list of cellular factors that are targeted for degradation by HIV-1 Vpr. Interestingly, the coexpression of GSN with HIV-1 NL4-3 resulted in the dose-dependent inhibition of gp160 and gp120 Env protein expression intracellularly, and this was paralleled by the reduction of virus-associated Env protein and the inhibition of viral infectivity. The effect of GSN on the infectivity of Vpr-deficient virus was reversed by the coexpression of Vpr *in trans*. Of note, the effect of GSN on viral infectivity was also reversed by the coexpression of the Vesicular stomatitis virus G (VSVg) protein *in trans*, suggesting that the loss of infectivity was likely due to the reduced amounts of virion-associated Env protein. Our data indicate that GSN accelerated the lysosomal degradation of the Env protein. We also found that GSN reduced the expression of VSVg, suggesting that the activity of GSN is not limited to HIV-1 Env but can affect the expression of other viral envelope proteins as well.

## RESULTS

**Identification of GSN as a Vpr binding protein in THP-1 cells.** To study the importance of Vpr in HIV-1 replication, we infected a set of T-cell lines and monocytic cells using wild type or Vpr-deficient HIV-1 virus stocks. Of the cell types analyzed, only primary human macrophages and differentiated THP-1 cells restricted Vpr-defective HIV-1 replication (Fig. 1, red) (29), whereas virus replication in all other cell types showed little to no Vpr-dependence (Fig. 1, blue). Unlike primary macrophages, immortalized THP-1 cells can easily be grown in large quantities and differentiated into macrophage-like cells via PMA treatment. Thus, we decided to use cell extracts from differentiated THP-1 cells to identify novel Vpr-interacting host factors that may inhibit replication if not counteracted by Vpr. The experimental strategy is schematically outlined in Fig. 2. As Vpr is known to degrade some of its cellular binding partners, we first expressed Flag-tagged Vpr in HEK293T cells (Fig. 2, step 1 and Fig. 3A), and we enriched Flag-Vpr from transfected cell extracts via immobilization on Flag affinity gel (Fig. 2, step 2) to avoid the premature degradation of Vpr-interacting host factors in THP-1 cells. As a specificity control, we employed a Flag-tagged segment of GFP, namely, GFP-N-Flag, which encoded the N-terminal 94 amino acids of EGFP downstream of the triple Flag tag. This construct was designed to yield a protein that was similar in size to Flag-Vpr and was enriched from transfected HEK293T cells in parallel (Fig. 3A). Curiously, both the Flag-tagged GFP-N and the Vpr proteins ran as doublets

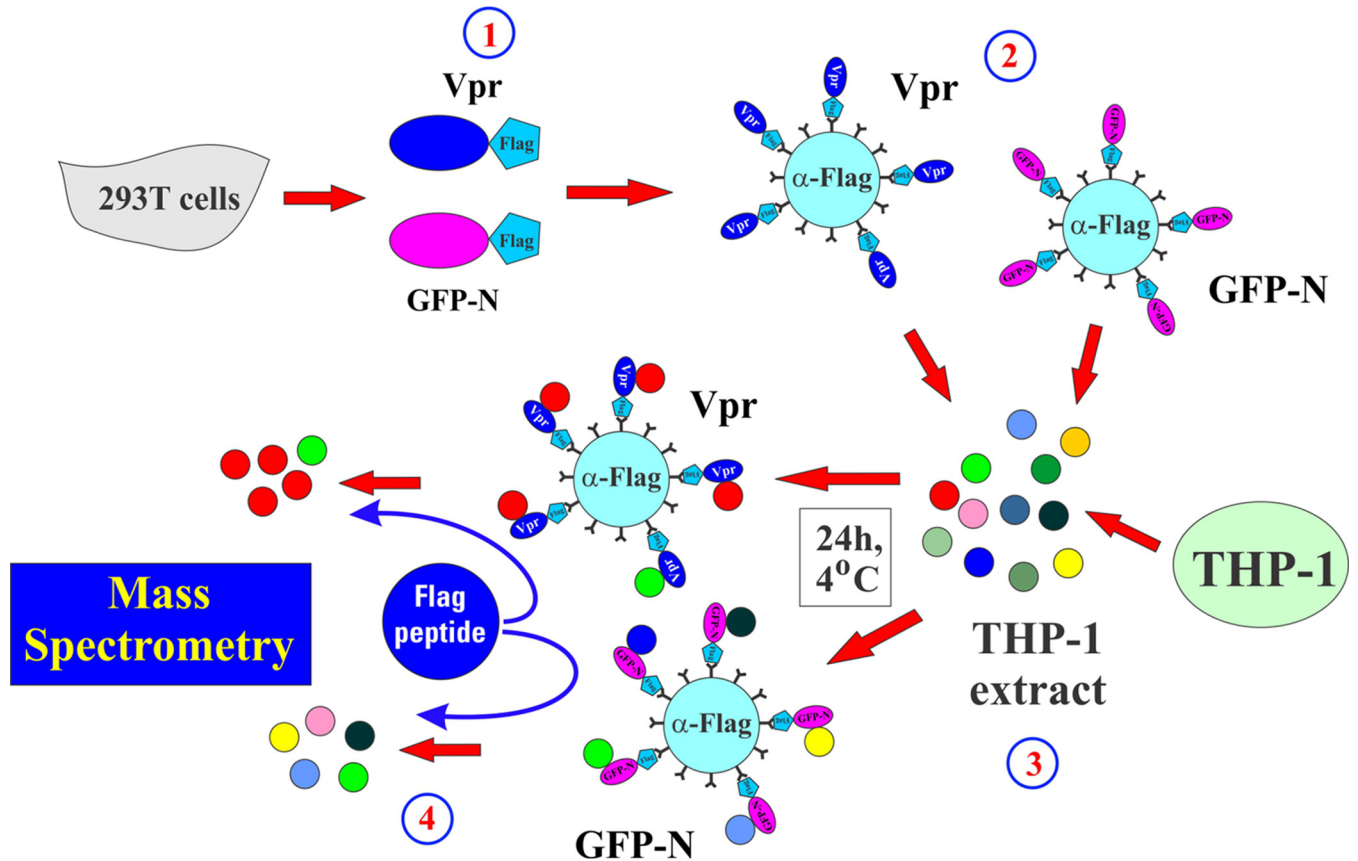


**FIG 2** Schematic depiction of the strategy employed for the identification of Vpr interacting proteins in differentiated THP-1 cells. Details are described in Materials and Methods. Flag-tagged Vpr and Flag-tagged GFP-N (which served as a negative control) were produced in transiently transfected HEK293T cells (step 1). Vpr-Flag and GFP-N-Flag proteins were immobilized on anti-Flag affinity gel and beads were washed extensively (step 2). Extracts from differentiated THP-1 cells were then exposed to the Vpr-Flag and GFP-N-Flag beads for 24 h at 4°C on a rotating platform (step 3). Unbound proteins were removed via the extensive washing of the affinity gel. Bound proteins were then released from the affinity gel via the addition of Flag peptide, and the eluted proteins were subjected to mass spectrometry (step 4).

on the gel (Fig. 3A). The reason for this is not clear, but we can rule out internal initiation, as the immunoblot employed an antibody against the N-terminal Flag epitope tag. Immobilized Vpr and GFP-N proteins, as well as plain Flag affinity beads (mock), were then exposed to cell extracts from  $1.5 \times 10^8$  PMA-treated THP-1 cells per sample for 20 h at 4°C on a rotating platform (Fig. 2, step 3). Bound proteins were eluted using Flag peptide and were processed for mass spectrometry (Fig. 2, step 4). The results from the mass spectrometric analysis were weighted based on the large number of peptides in the Vpr sample as well as the high normalized ratio of peptides recovered in the Vpr, compared to the GFP-N pulldown, and their relative abundance in the GFP-N pulldown. Proteins enriched by the Vpr bait that were not present at all or were present to a significantly lesser extent in the GFP-N pulldown were considered for further characterization. Overall, we identified 700 proteins that bound to GFP-N and 822 proteins that bound to Vpr (Fig. 3B). Of those, 353 proteins bound to GFP-N alone (Fig. 3B, turquoise), and 475 proteins bound to Vpr alone (Fig. 3B, pink), whereas 347 proteins bound to both Vpr and GFP-N (Fig. 3B, yellow). A plot of the results is shown in Fig. 3C, and an annotated table is available in Fig. S1. Proteins that were previously identified in connection with Vpr (i.e., DDB1, VPRBP, gelsolin [GSN]) are indicated in red, with a corresponding red dot next to the row in Fig. S1.

The fact that known Vpr-interacting proteins, such as DDB1 and VprBP (DCAF1), were identified in our screen with high scores suggested that our strategy for the identification of Vpr-interacting proteins was valid. One protein identified with a high score was GSN. Interestingly, GSN had previously been reported in connection with Vpr.

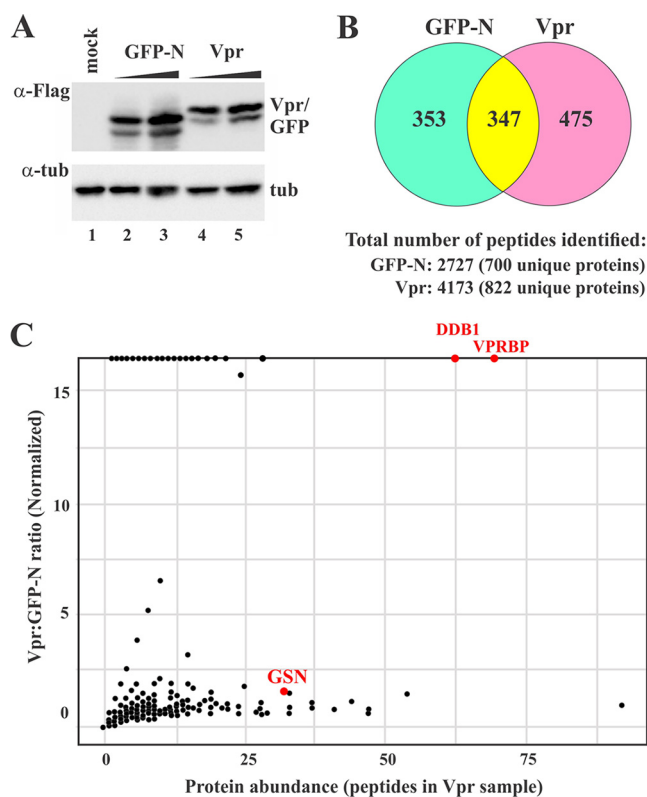


**FIG 3** Identification of Vpr-interacting proteins by mass spectrometry. Pulldown analysis for the identification of Vpr-interacting proteins from differentiated THP-1 cells. (A) Flag-tagged Vpr and Flag-tagged GFP-N were produced in transiently transfected HEK293T cells. An immunoblot analysis verified that both proteins were expressed with similar efficiency. Tubulin served as an internal control for sample loading. Lane 1, mock-transfected cells; lanes 2 and 4, 2  $\mu$ g plasmid DNA each; lanes 3 and 5, 4  $\mu$ g plasmid DNA each. (B) Venn diagram of the results of the mass spectrometry. Number of proteins and peptides identified in the GFP-N (turquoise) and Vpr (pink) pulldowns are shown. The yellow area symbolizes the overlap between the GFP-N and Vpr pulldowns. The proteins bound to Vpr were identified on average by five peptides (4,173 peptides over 822 proteins). (C) The protein abundance (number of peptides in Vpr sample; x axis) was plotted against the normalized Vpr:GFP-N ratio (y axis). The known Vpr-interacting proteins VPRBP, DDB1, and GSN are identified in red.

Specifically, it was reported that GSN inhibited Vpr-induced T-cell apoptosis by inhibiting the binding of Vpr to the voltage-dependent anion channel (VDAC) (27); however, mechanistic details remained unclear. Therefore, we decided to explore the functional consequences of the Vpr/GSN interaction in more detail, especially during the infection of monocytic cells in which Vpr is necessary for infection. First, we verified the association of Vpr with GSN via coimmunoprecipitation (Fig. 4). HEK293T cells were transfected with a vector expressing untagged NL4-3 Vpr together with either Flag-tagged GSN or Flag-tagged GFP-N. Initial attempts to demonstrate the Vpr-GSN interaction by co-IP using wild type Vpr were inconclusive, and this was presumably due to the concurrent proteasomal degradation of the Vpr-GSN complexes (data not shown). As the Vpr binding targets are often degraded through the interaction of Vpr and DCAF1, we used the DCAF1 binding mutant of NL4-3 Vpr (Vpr<sub>Q65R</sub>) in our co-IP experiment. Using Vpr<sub>Q65R</sub> we were able to demonstrate the Vpr/GSN interaction (Fig. 4, lane 10). The Flag-GFP-N IP produced a faint band of Vpr<sub>Q65R</sub> suggesting some degree of nonspecific interaction (Fig. 4, lane 12). Nevertheless, the Flag-GSN pulldown resulted in a clear enrichment of Vpr, compared to the Flag-GFP-N pulldown, attesting to the specificity of the interaction of Flag-GSN and Vpr<sub>Q65R</sub>. We also attempted to perform the reverse experiment (i.e., the co-immunoprecipitation of untagged GSN with Flag-tagged Vpr). However, those experiments produced a high background in the region where GSN would be expected to run and were thus inconclusive (data not shown).



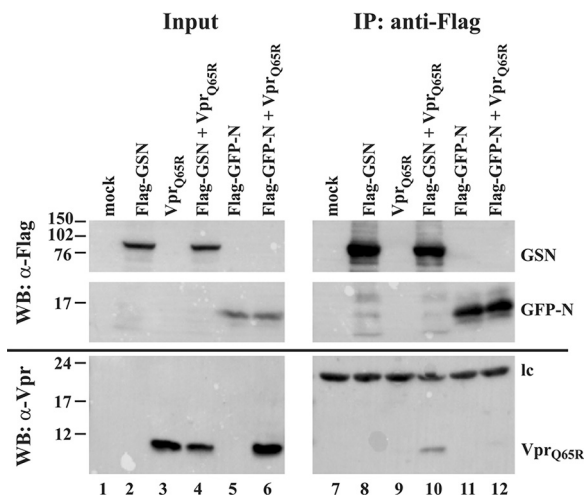


**FIG 4** One of the proteins identified in our proteomics screen was GSN. To confirm the specificity of the Vpr:GSN interaction, we performed a pulldown experiment using Flag-tagged GSN and, as a control, Flag-tagged GFP-N as baits for the pulldown of untagged NL4-3 Vpr<sub>Q65R</sub>. All proteins were expressed in the backbone of pVR1012 (51). Lanes 1 to 6 show input material identified by immunoblotting using Flag- (top) or Vpr-specific (bottom) antibodies. Proteins pulled down by Flag affinity gel and identified by immunoblotting are shown in lanes 7 to 12. Proteins are identified on the right. I $\kappa$ B, immunoglobulin light chain. This experiment was conducted three times, and a representative result is shown.

**GSN protein is expressed in human myeloid cells.** GSN is an important regulator of actin filament assembly and disassembly (for review, see [19, 30, 31]). Studies in mice have shown that murine GSN is expressed in most cell types but is downregulated in many cancer cells (21–24). We analyzed the expression of GSN in a variety of human cell types, including commonly used HIV-1 susceptible transformed T cell lines, primary human PBMC, MDM, HeLa cells, and HEK293T cells (Fig. 5A). We produced an antibody directed against the C-terminal 266 residues of GSN, as described in Materials and Methods. Somewhat surprisingly, the GSN protein was detectable only in MDM, THP-1, and PBMC (Fig. 5A). None of the other tested cell types produced a measurable amount of GSN protein. To see whether the expression of GSN was inducible via IFN treatment, uninfected MDM were treated with IFN- $\alpha$  for 48 h, and this was followed by immunoblotting with antibodies to GSN (Fig. 5B, [+]). Untreated extracts served as a reference (Fig. 5B, [–]). Tubulin served as an internal control for sample loading. We also probed for known IFN-inducible proteins (i.e., APOBEC3G [A3G] [32] and APOBEC3A [A3A] [33]). The results indicate that GSN expression is not regulated by IFN but is constitutively expressed in a cell type-specific manner.

**GSN is degraded by Vpr.** The fact that we were able to demonstrate the interaction of GSN with Vpr<sub>Q65R</sub> in Fig. 4 via co-IP but failed to demonstrate the interaction with wild type Vpr could be an indication that GSN, like many other Vpr-interacting proteins, is targeted for proteasomal degradation in the presence of wild type Vpr. To test this, we first cotransfected HEK293T cells with GSN with increasing amounts of either wild type Vpr (WT) or a DCAF1 binding mutant (Q65R) that is unable to induce the proteasomal degradation of Vpr-interacting factors (34). We consistently found that the steady-state levels of GSN were reduced in a dose-dependent manner in the presence of WT Vpr but not the Q65R mutant, even though the latter was expressed at somewhat higher levels (Fig. 6A). Quantitation of the GSN signal from three independent experiments showed that the reduction of GSN in the presence of WT Vpr was reproducible and approached statistical significance (Fig. 6A, right;  $P = 0.07$ ). This effect was not limited to NL4-3 Vpr (Fig. 6B, lanes 1 to 3), but it was also observed for Vpr from SIVcpz (Fig. 6B, lanes 4 to 6). Furthermore, the inhibition of GSN expression by Vpr was detected in both HeLa and HEK293T cells (Fig. 6B). In all cases, the quantitation of GSN from three independent analyses revealed the statistical significance of the

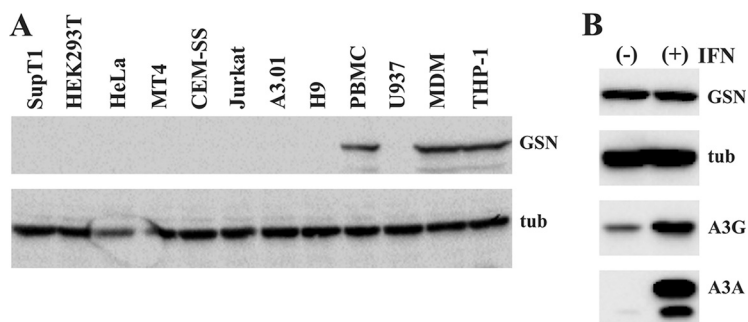


**FIG 5** Expression of GSN is cell type specific. (A) To assess GSN protein expression, extracts from various cell types were probed by immunoblotting with a GSN-specific antibody. The same blot was also probed with a tubulin-specific antibody, which served as a loading control. MDM and PBMC were from the same donor. (B) Terminally differentiated MDM from a healthy donor were either treated for 48 h with IFN- $\alpha$  (10 ng/mL; [+] IFN) or left untreated ([-] IFN). IFN- $\alpha$ -2A was from Sigma (cat. number GF416; shipped as a 1000 $\times$  solution in PBS) and was further diluted in PBS to the appropriate concentrations immediately before use. Whole-cell extracts were analyzed by immunoblotting using antibodies to GSN, tubulin (tub), APOBEC3G (A3G), and APOBEC3A (A3A). A3G and A3A are known IFN-inducible host proteins and were included as positive controls. Tubulin served as a loading control. The experiment was conducted three times with MDM from three different donors, and consistent results were obtained. A representative blot is shown.

Vpr-induced inhibition of GSN expression (Fig. 6B; graphs). Taken together, these results indicate that Vpr induces the degradation of GSN in transfected HEK293T and HeLa cells.

To directly demonstrate the involvement of the proteasomal pathway in the Vpr-induced degradation of GSN, we performed a pulse/chase experiment using untagged GSN and untagged NL4-3 Vpr (Fig. 6C). HEK293T cells were transfected with 0.5  $\mu$ g of pVR-GSN and 2.5  $\mu$ g of pVR-Vpr<sub>NL4-3</sub>. Approximately 24 h later, the cells were pulse-labeled for 15 min with [<sup>35</sup>S]-Expres<sup>35S</sup>-label (Perkin Elmer) and chased for 0, 15, 30, or 60 min in the absence (DMSO) or presence of MG132 (10  $\mu$ M), as detailed in Materials and Methods and in the figure legend. The cell extracts from all time points were immunoprecipitated with a GSN-specific antibody. The immunoprecipitated proteins were separated by SDS-PAGE, visualized by fluorography (Fig. 6C; top), and quantified as described in Materials and Methods. The quantitation of GSN from three independent experiments is shown at the bottom. The results show that treatment with the proteasome inhibitor MG132 stabilized the GSN levels (Fig. 6C, compare the red and blue curves), further supporting our conclusion that the Vpr-dependent reduction of GSN levels involves the proteasomal degradation of GSN.

**GSN reduces HIV-1 Env expression and incorporation into virus particles and reduces viral infectivity.** To examine the effects of GSN on virus production and infectivity, we transfected HEK293T cells with wild type or Vpr-defective pNL4-3 together with increasing amounts of untagged GSN vector. Cells and virus-containing supernatants were collected 24 h posttransfection and processed for immunoblotting using antibodies to Env (gp160, gp120), HIV-Ig (CA, p55), GSN, or tubulin (tub). A representative result of three independent transfections is shown (Fig. 7A). There was no noticeable effect of GSN on intracellular Gag protein synthesis or virus production (Fig. 7A, CA, p55). Interestingly, GSN expression reduced Env protein synthesis and packaging in a dose-dependent manner. We quantified cell-associated (Fig. 7B) and virus-associated Env levels (Fig. 7C) that had been corrected for variations in corresponding Gag levels from three independent experiments, and we found that, whereas the change in cell-associated Env did not reach statistical significance, the GSN-induced change in virus-associated Env levels was indeed statistically significant (Fig. 7C). Both gp160 and gp120 levels decreased as GSN expression increased (Fig. 7A, gp160, gp120) suggesting that the effect of GSN was at the level of Env synthesis or turnover, rather than Env maturation. Of note, virus preparations produced from transfected HEK293T cells contained variable amounts of unprocessed gp160 (e.g., compare Fig. 7A versus Fig. 8A). It

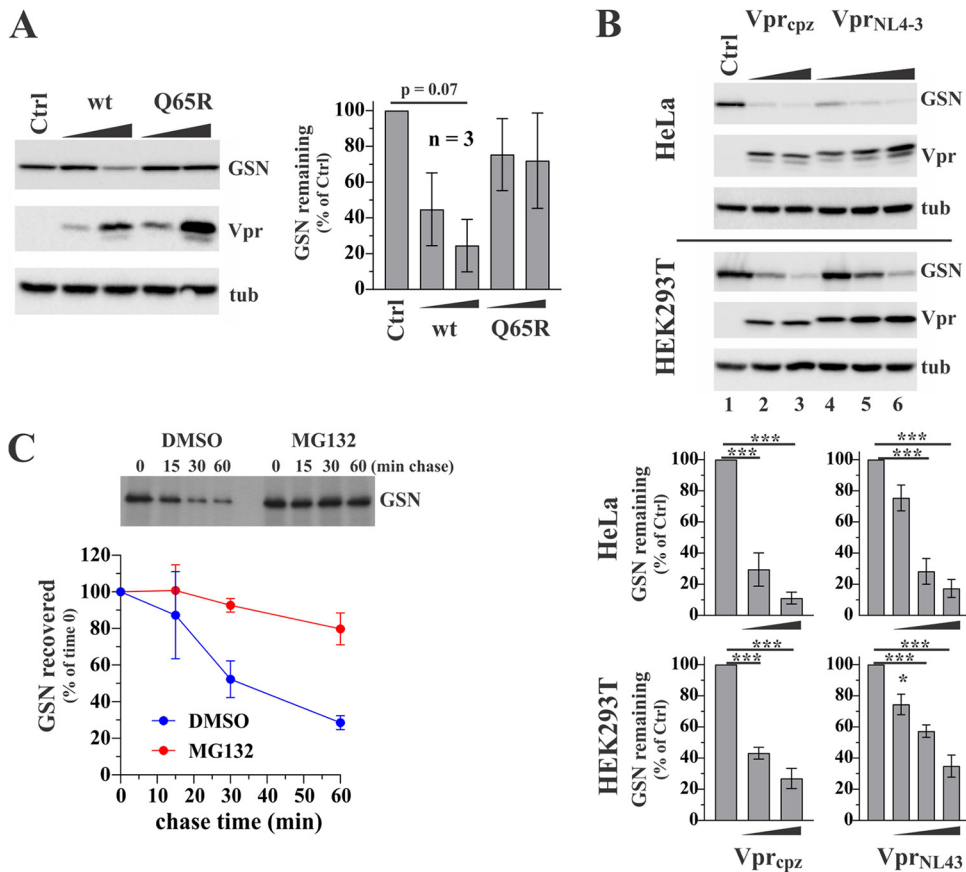


**FIG 6** The exogenous expression of Vpr inhibits GSN expression. (A) HEK293T cells ( $3 \times 10^6$ ) were transfected with 1  $\mu$ g of a vector expressing N-terminally Flag-tagged GSN, either in the absence of Vpr (Ctrl) or in the presence of increasing amounts (0.2 or 1  $\mu$ g) of Flag-tagged wild type Vpr (WT) or the DCAF1 binding mutant Vpr<sub>Q65R</sub>. The total amounts of transfected DNA were adjusted to 5  $\mu$ g using empty vector DNA. Cells were harvested 24 h after transfection. Whole-cell extracts were processed for immunoblotting using antibodies to the Flag epitope, recognizing both GSN and Vpr, as well as tubulin. Proteins are identified on the right. A representative of three independent experiments is shown. Quantitation of the GSN levels was done using Fujifilm Multi Gauge software. The results were graphed using GraphPad Prism (v9.4.1). The error bars represent the standard error of the mean of three experiments. Statistical significance was analyzed in GraphPad Prism, using an ordinary one-way ANOVA and a *post hoc* Dunnett's test. *P* values are depicted as \*, *P* < 0.05; \*\*, *P* < 0.01; \*\*\*, *P* < 0.001. (B) HeLa (top) and HEK293T cells (bottom) were transfected with N-terminally Flag-tagged GSN (1  $\mu$ g) together with 5  $\mu$ g of empty vector DNA (Ctrl) or increasing amounts (2.5 and 5  $\mu$ g) of untagged SIVcpzEK505 Vpr (Vpr<sub>cpz</sub>) or increasing amounts (1, 2.5, 5  $\mu$ g) of untagged NL4-3 Vpr (Vpr<sub>NL4-3</sub>). The total amounts of transfected DNAs were adjusted to 6  $\mu$ g using empty vector DNA. Cells were harvested 24 h after transfection. Whole-cell extracts were processed for immunoblotting using antibodies to the Flag epitope (GSN), SIVcpz Vpr (Vpr), or tubulin (tub). Proteins are identified on the right. Note that the antibody to Vpr from SIVcpz efficiently cross-reacts with NL4-3 Vpr. The experiments were conducted three times each, and the amounts of GSN remaining in the presence of increasing amounts of Vpr were calculated and presented as in panel A. The results are shown at the bottom of panel B. The error bars represent the standard error of the mean of three independent experiments each. Statistical significance was analyzed in GraphPad Prism, using the same methods as described in panel A. In all cases, the reduction of GSN expression by Vpr was statistically significant. (C) For metabolic labeling, HEK293T cells were transfected with 0.5  $\mu$ g of untagged pVR-GSN and 2.5  $\mu$ g of untagged pVR-Vpr<sub>NL4-3</sub>. Empty vector (1.5  $\mu$ g) was added to adjust the total amounts of transfected DNA to 5  $\mu$ g. 24 h after transfection, the cells were pulse-labeled for 15 min in the presence or absence of 10  $\mu$ M proteasome-inhibitor MG132 (Sigma-Aldrich; St. Louis, MO; cat. number M7449) and chased for 0, 15, 30, or 60 minutes. MG132 was present during the starvation period, the labeling period, and the chase period. An equivalent volume of DMSO was added to the control samples. GSN from each time point was immunoprecipitated with an antibody to GSN and analyzed via fluorography, using a Typhoon FLA 9500 Phosphorimager, as described in Materials and Methods. GSN specific bands were quantified using Fujifilm Multi Gauge software, as described for panel A. The error bars represent the standard error of the mean of three independent experiments and was calculated using GraphPad Prism software.



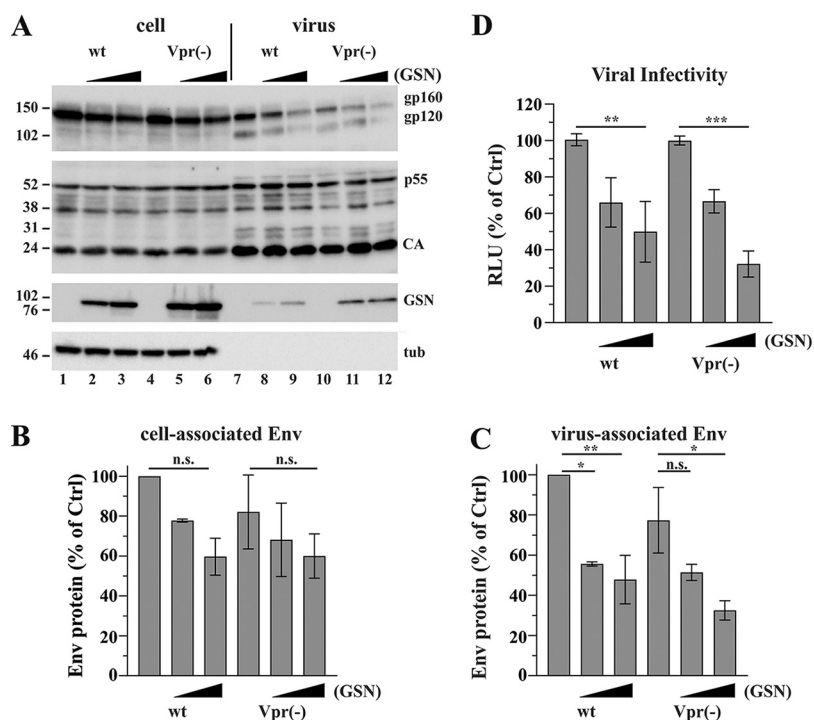


**FIG 7** GSN-induced inhibition of Env expression attenuates HIV-1 infectivity. (A) HEK293T cells were transfected with 4  $\mu$ g of either wild type pNL4-3 (WT) or pNL4-3 Vpr (-) (Vpr [-]) in the absence of GSN (lanes 1 and 4) or increasing amounts of untagged GSN (lanes 2 and 5: 0.3  $\mu$ g; lanes 3 and 6: 1  $\mu$ g). Cells and virus-containing supernatants were collected 24 h after transfection. Whole-cell extracts (lanes 1 to 6) and concentrated viral supernatants (lanes 7 to 12) were processed for immunoblot analysis and probed with antibodies to gp120 (gp160, gp120), HIV-Ig (p55, CA), GSN, or tubulin (tub). Proteins are identified on the right. Molecular weight standards are shown on the left. A representative result of three independent experiments is shown. Cell-associated Env (B) and virus-associated Env (C) from three independent experiments were quantified using Fujifilm Multi Gauge software, as described in Materials and Methods, and graphed as a percentage of the control (no GSN), using GraphPad Prism software. All signals were corrected for variations in CA levels. Statistical significance was analyzed in GraphPad Prism, using an ordinary one-way ANOVA and a *post hoc* Sidak's test. *P* values are depicted as \*, *P* < 0.05; \*\*, *P* < 0.01; n.s., not significant. (D) Viral infectivity was determined using filtered, unconcentrated supernatants from three independent transfections (panel A) by infecting TZM-bl cells in triplicate (i.e., a total of nine wells for each condition). Virus-induced luciferase activity was determined 48 h later. Results were corrected for variations in the input RT values and expressed as percentages of the signal obtained in the absence of GSN, which was defined as 100%. Results show the mean of nine data points each, and error bars reflect the standard error of the mean. Statistical significance was analyzed in GraphPad Prism, using an ordinary one-way ANOVA and a *post hoc* Sidak's test. *P* values are depicted as \*\*, *P* < 0.01; \*\*\*, *P* < 0.001; n.s., not significant (*P* > 0.05).

is not clear to what extent unprocessed gp160 contributes to the infectivity of virus particles; however, we included both gp160 and gp120 in our quantitation of virus associated Env. To determine the impact of GSN on viral infectivity, virus-containing supernatants were used to infect TZM-bl cells. Tat-induced luciferase activity was measured 48 h later and was corrected for variations in input virus. We found that the GSN-induced reduction in Env expression was paralleled by a dose-dependent and statistically significant inhibition of viral infectivity, as indicated by the decreasing Tat-induced luciferase activity in TZM-bl cells (Fig. 7D). Because of our observation that Vpr induces the degradation of GSN (Fig. 6), we expected to see a less pronounced effect of GSN on the infectivity of the WT virus, compared to the Vpr-defective virus. However, while we did observe slightly reduced levels of GSN in cells expressing the WT virus (Fig. 7A, GSN blot: compare lanes 2 and 3 to lanes 5 and 6), this difference did not translate into differences in the inhibition of viral infectivity (Fig. 7D). Thus, whereas these experiments clearly established an inverse correlation for GSN and Env expression, the exact impact of Vpr on counteracting the inhibitory effect of GSN remained uncertain.

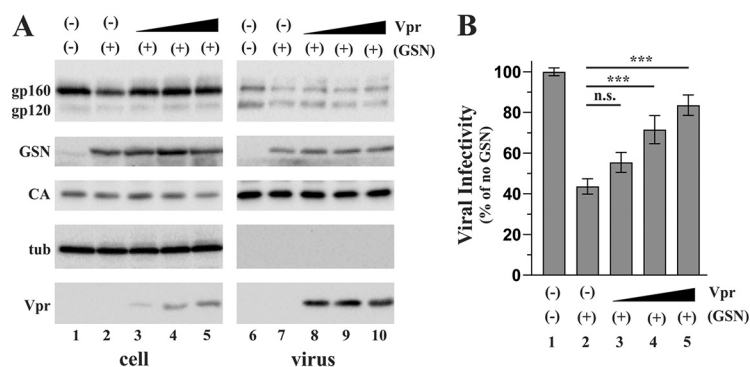


**FIG 8** Vpr rescues viral infectivity. HEK293T cells were transfected with 4  $\mu$ g of pNL4-3Vpr (-), either in the absence of GSN (lane 1) or together with 1  $\mu$ g of untagged pVR-GSN (lanes 2 to 5). Increasing amounts of untagged pVR-Vpr (0.1, 0.2, 0.3  $\mu$ g [lanes 3 to 5]) were added to the wells. The total amounts of DNA were adjusted to 6  $\mu$ g, using empty vector DNA as needed. Samples were harvested 24 h later and cells and virus-containing supernatants were processed for immunoblotting as described in Fig. 7. (A) Cell extracts and concentrated culture supernatants were separated by SDS-PAGE and probed with antibodies to gp120 (gp160, gp120), GSN, HIV-Ig (CA), tubulin (tub), or Vpr. Proteins are identified on the left. A representative result of five independent experiments is shown. (B) Virus-containing supernatants from five independent transfections were used to infect TZM-bl cells in triplicate (i.e., a total of 15 wells for each condition). Virus-induced luciferase activity was determined 48 h later. Results were corrected for variations in the input RT values and are expressed as percentages of the signal obtained in the absence of GSN, which was defined as 100%. The results show the mean of 15 infections, and the error bars reflect the standard error of the mean. Statistical significance was analyzed in GraphPad Prism, using an ordinary one-way ANOVA and a *post hoc* Sidak's test (comparing samples with GSN in the absence or presence of increasing Vpr levels). *P* values are depicted as \*, *P* < 0.05; \*\*, *P* < 0.01; \*\*\*, *P* < 0.001; n.s., not significant (*P* > 0.05).

**The GSN-mediated loss of viral infectivity is reversed by the expression of exogenous Vpr in trans.** The results from Fig. 7 indicate that GSN inhibits viral infectivity in a dose-dependent manner. However, there was no clear difference between the WT and Vpr-defective viruses, which we attributed to the low levels of virus encoded Vpr, relative to the exogenously overexpressed GSN. To test this hypothesis, we assessed the effect of increasing levels of exogenously expressed Vpr on the infectivity of Vpr-defective HIV-1 produced in the presence of constant amounts of GSN. For this purpose, Vpr-defective pNL-43 (4  $\mu$ g) was cotransfected with 1  $\mu$ g of untagged pVR-GSN and increasing amounts (0, 0.1, 0.2, 0.3  $\mu$ g) of untagged pVR-Vpr. Cells and virus-containing supernatants were collected 24 h later and processed for immunoblotting, using antibodies to Env (gp160/gp120), GSN, HIV Ig (CA), tubulin (tub), and Vpr (Fig. 8A). A representative blot from three independent experiments is shown. We observed a slight reduction in Env expression in the presence of GSN (Fig. 8A, Env blot: compare lanes 1 and 2), which went away upon the coexpression of Vpr. Cell-free supernatants were used to infect TZM-bl indicator cells, and the Tat-induced luciferase activity was measured 48 h later (Fig. 8B). Consistent with the results from Fig. 7D, GSN reduced the viral infectivity to about 40% of the GSN-deficient control (Fig. 8B, compare columns 1 and 2). Importantly, the co-expression of Vpr gradually restored viral infectivity in a dose-dependent and statistically significant manner. (Fig. 8B). Thus, Vpr has the ability to counteract the effect of GSN on viral infectivity.

**Gelsolin is not packaged into HIV-1 virions.** In Fig. 7A and 8A, we noticed the presence of GSN in cell-free supernatants, suggesting that GSN may be packaged into viral particles. Indeed, the packaging of GSN into HIV-1 virions could offer an alternative explanation for its inhibitory effect on viral infectivity. GSN has been shown to exist in two isoforms, one of which (plasma gelsolin) is secreted into culture supernatants (17, 35). To address whether GSN is associated with HIV-1 virions, we performed OptiPrep density gradient analyses of concentrated supernatants from HEK293T cells expressing GSN in the absence or presence of WT HIV-1<sub>NL-43</sub> (Fig. S2A). Under the experimental conditions used, viral particles were enriched in fractions 6 to 8 of the

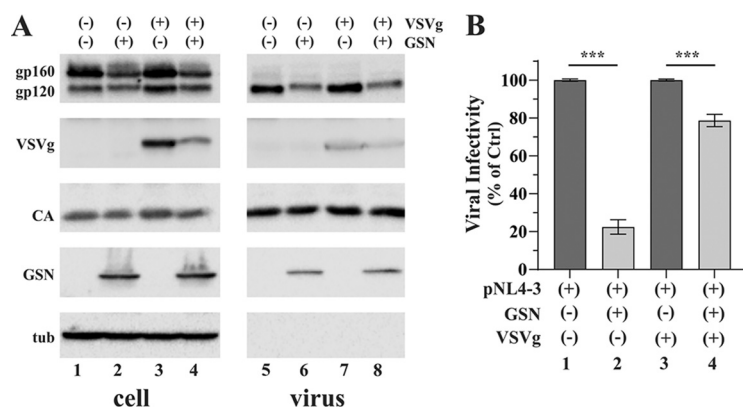


**FIG 9** The inhibitory effect of GSN on viral infectivity can be rescued by pseudotyping with VSVg. (A) HEK293T cells were transfected with 4.0  $\mu$ g of pNL4-3Vpr (-) together with 1.5  $\mu$ g of either untagged GSN (lanes 2 and 4) or empty vector (lanes 1 and 3). For pseudotyping the virus, 0.5  $\mu$ g of VSVg vector was cotransfected (lanes 3 and 4). The amount of transfected DNA was adjusted to 6  $\mu$ g total DNA in all samples. Cells and virus-containing supernatants were collected 24 h later and processed for immunoblotting. Cell lysates (cell) and concentrated viral extracts (virus) were separated by SDS-PAGE and probed with antibodies to Env (gp160, gp120), VSVg, HIV-Ig (CA), GSN, or tubulin (tub). Proteins are identified on the left. A representative result of three independent experiments is shown. (B) Virus infectivity was determined via the infection of TZM-bl cells in triplicate (i.e., a total of nine wells for each condition). The results were corrected for fluctuations in the input virus and virus infectivity observed in the absence of GSN, which was defined as 100% for each experimental set. The results are shown as an average of three independent experiments along with standard error of the mean. Statistical significance was analyzed in GraphPad Prism, using an ordinary one-way ANOVA and a *post hoc* Sidak's test. *P* values are depicted as \*, *P* < 0.05; \*\*, *P* < 0.01; \*\*\*, *P* < 0.001.

gradient, as indicated by the red box. In contrast, GSN revealed a much broader distribution and was found in fractions 1 to 8 of the gradient, without an apparent enrichment in the viral fractions. Indeed, the distribution of GSN in the gradient did not change in the presence of the virus. These results suggest that GSN is secreted from transfected HEK293T cells but is not incorporated into viral particles.

**VSVg neutralizes the effect of GSN on viral infectivity.** If the loss of infectivity observed in Fig. 7 in the presence of GSN is indeed due to the smaller amounts of virus-associated Env, it should be possible to compensate for the lower infectivity by pseudotyping viral particles with VSVg glycoprotein. To test this hypothesis, Vpr-defective NL4-3 virus was produced in HEK293T cells in the presence or absence of GSN as well as in the presence or absence of VSVg (Fig. 9). Transfected cells and virus-containing supernatants were collected 24 h later and processed for immunoblotting. Membranes were probed with antibodies to Env (gp160, gp120), VSVg, HIV-Ig (CA), GSN, or tubulin (tub) (Fig. 9A). A representative result from three independent experiments is shown. As before, the expression of GSN had no effect on cell- or virus-associated Gag levels, but it did reduce cell-associated gp160 and gp120 as well as virus-associated gp120 levels (Fig. 9A, top panels). As expected, GSN expression reduced viral infectivity in the absence of VSVg (Fig. 9B, compare columns 1 and 2). However, pseudotyping with VSVg clearly restored viral infectivity, even though the difference between the absence and presence of GSN remained statistically significant (Fig. 9B, compare columns 3 and 4). Since VSVg did not affect the expression or secretion of GSN (Fig. 9A, compare lanes 2 and 4 and lanes 6 and 8), these results support the notion that the loss of infectivity induced by GSN overexpression is due to its effect on Env packaging.

**Reduced Env expression is not due to the differential splicing of viral mRNA.** There are two possible ways for GSN to reduce the expression of Env without affecting the overall expression of viral proteins, such as Gag: (i) GSN could affect the splicing pattern that would affect the relative abundance of alternatively spliced mRNAs. For instance, we previously observed such an effect when the mutation of the Vpu initiation codon increased Env expression from its downstream AUG on the bicistronic Vpu/Env mRNA (36). Indeed, a minimal uORF within the HIV-1 vpu leader allows for the

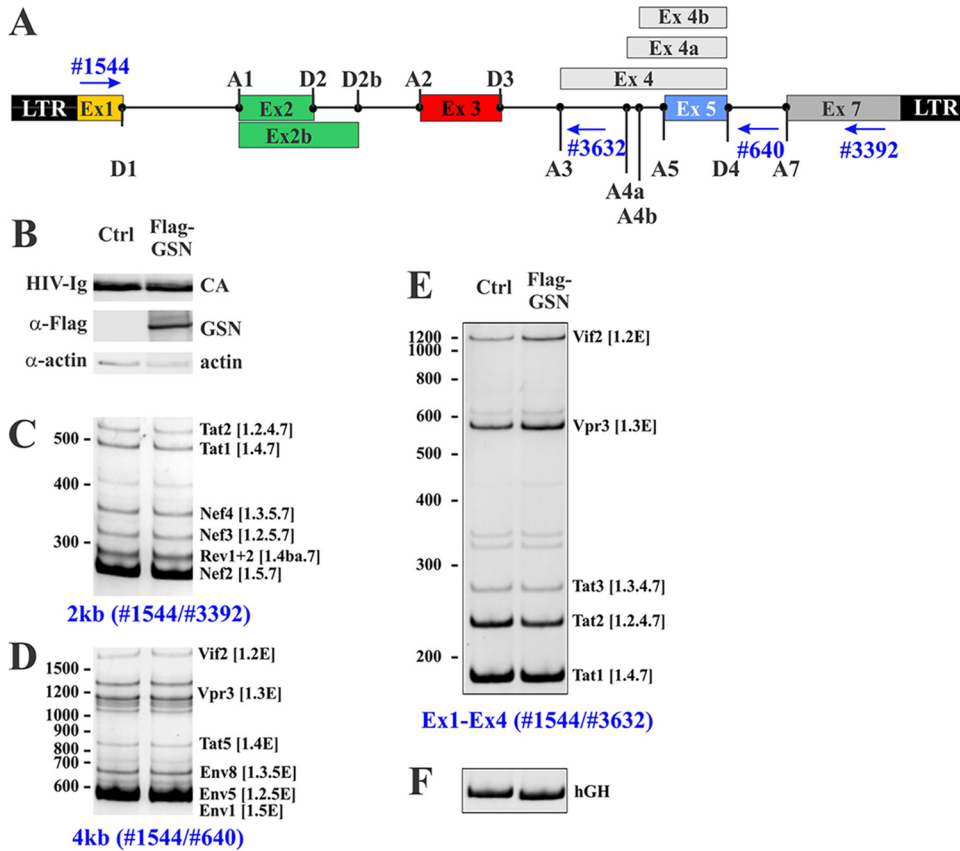


**FIG 10** Influence of GSN overexpression on the HIV-1 splicing pattern. (A) Illustration of the HIV 1 proviral genome, including viral LTRs, HIV-1 exons, and 5' and 3' splice sites. The location of the primer binding sites #1544, #640, #3632, and #3392 used in the analysis are indicated. (B) Immunoblot analysis of HIV-1 p24 CA protein expression. HEK293T cells were transfected with pNL4-3, pXGH5, and Flag-GSN. The p24 CA protein levels and the exogenous expression of Flag-GSN were determined using anti-p24 CA and anti-FLAG antibodies. The detection of actin served as a loading control. (C–F) RT-PCR analysis of RNAs isolated from cells in panel B. Technical details are described in Materials and Methods. The following primer pairs were used: (C) #1544/#3392 (2 kb species), (D) #1544/#640 (4 kb species), and (E) #1544/#3632 (Ex1-4 splicing). The HIV-1 mRNA species, according to Purcell and Martin (52), are indicated on the right of each gel image. Exon numbers are indicated in square brackets. (F): The detection of human growth hormone (hGH) mRNA served as a transfection control. The splice pattern analysis was done twice, and identical results were obtained.

initiation of efficient translation at the downstream env AUG (37). (ii) GSN could increase the turnover of the Env protein, for instance, by redirecting it to lysosomes for degradation. We first tested the possible effects of GSN on mRNA splicing. HIV-1 genes are expressed from a common mRNA precursor that is spliced into a series of subgenomic mRNAs that encode individual viral genes (Fig. 10A). We compared the viral mRNA splicing pattern in cells producing NL4-3 either in the absence of GSN (Fig. 10C to E, Ctrl) or in the presence of Flag-tagged GSN (Fig. 10C to E, Flag-GSN). A portion of the cells was processed for immunoblotting (Fig. 10B) to document Gag (CA) and GSN expression ( $\alpha$ -Flag). Actin served as an internal control for sample loading.

mRNA was isolated from the remaining cells, and an RT-PCR analysis was performed using specific primer pairs (indicated by blue arrows in Fig. 10A). No difference in the splicing pattern of any intronless HIV-1 mRNA that coded for Tat, Rev, or Nef could be detected, suggesting comparable overall viral gene transcription (Fig. 10C) (2 kb mRNAs, #1544/#3392). The same was true for the intron-containing *vif*, *vpr*, one-exon *tat* (Tat5), or *env* coding mRNAs (Fig. 10D) (4 kb mRNAs, #1544/#640), suggesting that *env* mRNA expression was not altered by GSN. Consistent with this, an analysis of the noncoding leader of the 4 kb HIV-1 messages (Fig. 10E) (#1544/#3632) also showed no evidence for an altered splicing pattern by GSN that could have affected *env* mRNA

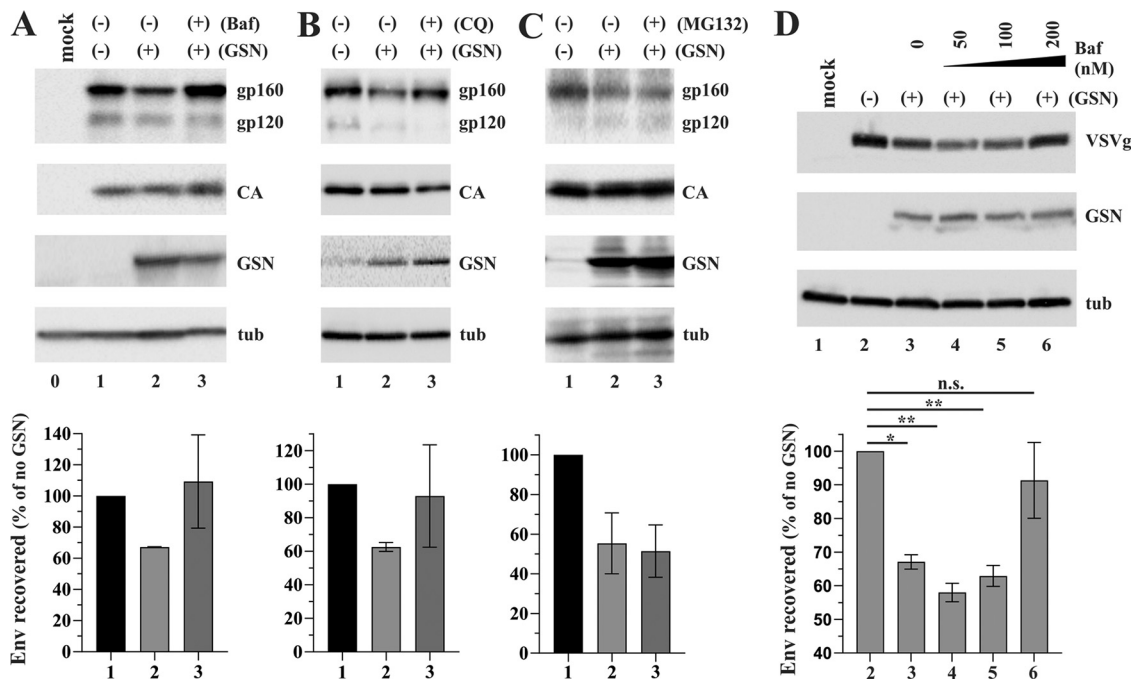


**FIG 11** Lysosomal inhibitors antagonize the effect of GSN and restore levels of HIV-1 Env and VSVg. (A–C) HEK293T cells were transfected with 4.0  $\mu$ g of pNL4-3 together with 1  $\mu$ g of either untagged GSN (lanes 2 and 3) or empty vector (lane 1). A mock transfected sample was included in panel A (lane 0). 20 hours after transfection, the cells were treated for 4 h each with 50 nM Bafilomycin (Baf; panel A, lane 3), 10  $\mu$ M chloroquine (CQ) (panel B, lane 3), or 8 h with 10  $\mu$ M MG132 (panel C, lane 3). All other samples received equivalent volumes of DMSO as a carrier control (lanes 1 and 2). (D) HEK293T cells were transfected with 0.5  $\mu$ g of pCMV-VSVg and 1.5  $\mu$ g of either untagged GSN (lanes 3 to 6), or empty vector (lane 2). The total amounts of transfected DNA were adjusted to 5  $\mu$ g in all samples. 20 hours after transfection, cells were treated for 4 h each, with increasing amounts of Bafilomycin (Baf; 0 to 200 nM as indicated). (A–D) Following inhibitor treatment, the cells were collected and processed for immunoblotting as detailed in Materials and Methods. Cell lysates were separated by SDS-PAGE. Membranes from panels A to C were probed with antibodies to Env (gp160/gp120), HIV Ig (CA), GSN, and tubulin (tub). Membranes from panel D were probed with antibodies to VSVg, GSN, or tubulin. Proteins are identified on the right. The experiments were independently conducted twice (panels A, B, and D) or three times (panel C). Env proteins were quantified and analyzed as described in Fig. 7. The error bars represent the standard error of the mean. The statistical significance in panel D was analyzed in GraphPad Prism, using an ordinary one-way ANOVA and a *post hoc* Tukey's test. *P* values are depicted as \*, *P* < 0.05; \*\*, *P* < 0.01; n.s., nonsignificant (*P* > 0.05).

production. Thus, we conclude that GSN has no effect on the splicing pattern of HIV-1 mRNAs in GSN-transfected HEK293T cells.

**GSN targets both HIV-1 Env and VSVg glycoproteins for lysosomal degradation.** Next, we tested the possibility that GSN contributed to the enhanced lysosomal degradation of Env. To do so, HEK293T cells were transfected with Vpr-deficient pNL4-3 in either the absence or the presence of GSN (Fig. 11). To maximize the effects of GSN, the Vpr-deficient virus was used here. Treatment with either lysosomal or proteasomal inhibitors was done 20 h after transfection as follows. Cells were treated either with 50 nM bafilomycin (Fig. 11A; Baf [4 h]), 10  $\mu$ M chloroquine (Fig. 11B; CQ [4 h]), or 10  $\mu$ M MG132 (Fig. 11C; MG132 [8 h]). Control samples received comparable volumes of DMSO. Following inhibitor treatment, whole-cell extracts were prepared and processed for immunoblotting, using antibodies to HIV-1 Env (gp160, gp120), HIV-Ig (CA, p55), GSN, or tubulin (tub), with the latter serving as an internal reference for sample loading. The quantitation of Env from two or three independent experiments is shown at the bottom of each panel. All data points were corrected for differences in the corresponding CA signals. As before, the expression of GSN resulted in reduced levels of the Env protein, whereas the levels of HIV-1 Gag proteins (CA, p55) were largely unaffected. Importantly, treatment with either bafilomycin (Fig. 11A, lane 3) or chloroquine (Fig. 11B, lane 3) restored the levels of Env to those seen in the absence of GSN. In contrast, treatment with the proteasome inhibitor MG132 had no stabilizing effect (Fig. 11C, lane 3). The stabilizing effects of lysosomal inhibitor treatment are obvious



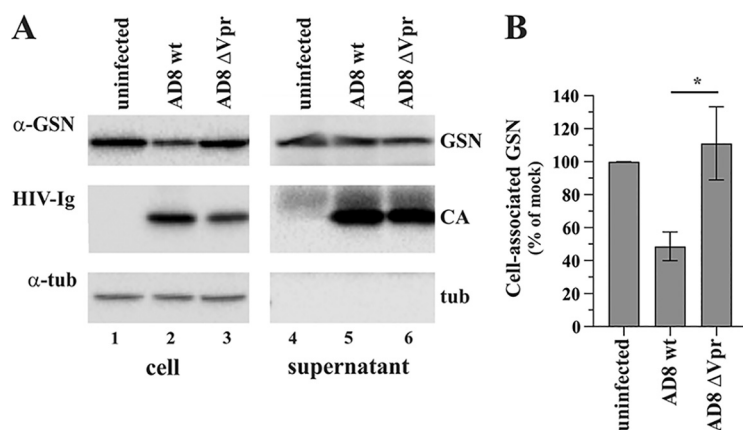


**FIG 12** Expression and secretion of endogenous GSN in HIV-infected MDM. MDM were infected with VSVg-pseudotyped virus stocks of wild type AD8 (lanes 2 and 5) or Vpr-deficient AD8 (lanes 3 and 6). Uninfected cells were cultured in parallel (lanes 1 and 4). (A) Cells and virus-containing supernatants were harvested 6 days postinfection and were processed for immunoblotting. Cell lysates (cell) and concentrated viral supernatants (virus) were separated by SDS-PAGE and probed with antibodies to GSN (GSN), HIV-Ig (CA), and tubulin (tub). Proteins are identified on the right. A representative of three independent experiments is shown. (B) Cell-associated GSN levels were quantified from three independent experiments using the Fuji Image Gauge software package and analyzed using the GraphPad Prism software package. The levels of GSN in the uninfected cultures were defined as 100% for each set of experiments. Statistical significance was analyzed in GraphPad Prism, using an ordinary one-way ANOVA and a *post hoc* Tukey's test. *P* values are depicted as \*, *P* < 0.05.

from the graphs at the bottom of each panel, even though the differences did not reach statistical significance due to the small sample size. Nevertheless, we can conclude that the reduction of Env expression in GSN-expressing cells likely results from the enhanced turnover of Env in lysosomes.

Similarly, we tested the effect of lysosomal inhibitor treatment on the GSN-induced inhibition of VSVg expression (Fig. 11D). HEK293T cells were transfected with pCMV-VSVg in the absence or presence of GSN. 24 h after transfection, cells were treated for 4 h with various concentrations of bafilomycin (Baf). Whole-cell extracts were then prepared and processed for immunoblotting, using antibodies to VSVg, GSN, or tubulin (tub). We found that increasing amounts of bafilomycin increasingly restored VSVg levels in the cell extracts. Therefore, we conclude that GSN directs both HIV-1 Env and VSVg glycoproteins into a lysosomal degradation pathway. Thus, the effect of GSN is not exclusive to HIV-1 Env but can affect other membrane proteins, as well. The precise mechanism by which GSN accomplishes this task remains the subject of future investigations.

**Analysis of endogenous GSN in HIV-1 infected MDM.** In Fig. 6, we showed that the co-expression of Vpr and GSN led to the degradation of GSN. To assess the impact of HIV-1 infection on the expression of endogenous GSN in MDM, we infected MDM with either AD8 WT or AD8ΔVpr virus stocks. Uninfected cells were included for reference (Fig. 12A). Virus stocks were pseudotyped with VSVg to minimize the differences in viral protein synthesis that were caused by the reduced replication fitness of Vpr-deficient HIV-1 in macrophages (Fig. 1; MDM). Cells and virus-containing supernatants were collected 6 days postinfection and processed for immunoblotting, using HIV-Ig (CA), GSN, or tubulin (tub) (Fig. 12A). The levels of GSN from three independent infections using MDM from different donors were quantified (Fig. 12B). Indeed, the infection of MDM with WT HIV-1 AD8 showed significantly reduced cellular levels of endogenous GSN, compared to the Vpr-deficient virus. The GSN levels in cells infected with the Vpr-deficient virus were not significantly different from those observed in uninfected cells. As with the transfected HEK293T cells (Fig. 7 and 9), GSN was detected in the supernatants of all of the macrophage cultures, including the uninfected cultures. To assess whether endogenous GSN was associated with viral particles, we performed OptiPrep density gradient centrifugation of concentrated culture supernatants (Fig. S2B). GSN was readily detected in the OptiPrep gradients. However, as with the supernatants

from the transfected HEK293T cells, GSN partitioned with the low-density fractions of the gradients and failed to accumulate in the virus-containing fractions (Fig. S2B, red box). We conclude that endogenous GSN is secreted from both uninfected and infected macrophages but does not associate with HIV-1 virions.

## DISCUSSION

GSN is a host cell protein that is involved in the assembly and disassembly of actin filaments. Here, we identified GSN as a Vpr-interacting host factor through a proteomics screen of differentiated THP-1 cells. An analysis of GSN expression in various cell types revealed that the GSN protein was highly expressed in cells of myeloid origin (i.e., THP-1 and MDM) but was undetectable in all of the other cell types tested (Fig. 5A). This is consistent with reports on the downregulation of GSN expression in many cancer cells (21–24). As far as the role of GSN in HIV biology is concerned, a previous study showed that GSN overexpression protected cells from Vpr-induced T-cell apoptosis and interfered with the binding of Vpr to the voltage-dependent anion channel (VDAC) (27). However, this study focused on Jurkat and HEK293T cells, which we found to lack demonstrable expression of GSN. Indeed, our own coimmunoprecipitation studies revealed a physical interaction of GSN and Vpr that resulted in the degradation of transiently expressed GSN in HEK293T cells. Thus, our data are the first to identify GSN as a novel host factor that is targeted for degradation by Vpr.

GSN is expressed in two isoforms that are derived from the differential splicing of a common precursor and use different translation initiation sites (17, 18). Isoform 1 is also referred to as plasma GSN and was found at increased levels in the plasma of HIV-1-infected individuals (17, 35). Indeed, plasma GSN levels were suggested to be an indicator of inflammation and may serve as a diagnostic tool (reviewed in [38]). Isoform 2 lacks 51 amino acids at its N terminus, including a 27-residue signal peptide that is cleaved off the mature isoform 1. Both isoforms are assumed to coexist intracellularly. However, their relative abundances are difficult to determine, as they cannot easily be separated by gel electrophoresis due to their small difference in size. To bypass this problem, we designed vectors producing either isoform 1 or isoform 2 and found no difference in their effects on HIV-1 Env expression and packaging (not shown). Therefore, we treated the two isoforms as functionally equivalent and used isoform 1 for all of the experiments shown here. Of note, while both endogenously expressed GSN from macrophages as well as overexpressed GSN from transfected HEK293T cells was secreted into culture supernatants, irrespective of whether the cells were HIV-1-infected or not, GSN did not partition with viral fractions, suggesting that GSN does not get packaged into HIV-1 virions. Thus, all of the data presented in this study point to the stability of the viral Env protein as the relevant target of GSN activity.

Unfortunately, efforts to deplete endogenous GSN in MDM or THP-1 cells, using siRNA or CRISPR-Cas9 techniques to assess its impact on the replication of Vpr-defective HIV-1 in primary cells, were unsuccessful. In the case of THP-1 cells, cells lacking GSN failed to proliferate. The reasons are not entirely clear, as we were able to knock down the expression of other cellular genes in uninfected and infected cultures (data not shown). However, we did observe a reduction of endogenous GSN expression in HIV-infected MDM, compared to uninfected cells or cells infected with the Vpr-deficient virus (Fig. 12). It is interesting to note that the extent to which GSN levels are reduced by exogenously overexpressed Vpr in transfected HEK293T cells (Fig. 6) is not dramatically different from the effect observed in macrophages after an infection with Vpr-expressing HIV-1 (Fig. 12B). Nevertheless, the assessment of the overall impact of GSN on virus replication in myeloid cells is complicated by the fact that Vpr has been found to target other cellular factors, besides GSN. There are several published studies that report that Vpr stabilizes Env in HIV-1 infected MDM (39, 40). However, the mechanism of action remains under debate. For instance, the Collins lab reported that Vpr increases Env expression by degrading the myeloid-specific mannose receptor 1 protein (41), whereas the Zheng lab proposed an ER-associated degradation pathway (40).

The results from our own study implicate GSN in the regulation of HIV-1 Env expression. Thus, there may be multiple redundant mechanisms at play that affect viral infectivity in MDM.

Finally, the effect of GSN on HIV-1 Env expression is not exclusive. Indeed, we found that GSN also reduced the expression of VSVg and that this effect was reversed when cells were treated with lysosomal inhibitors. Therefore, our results suggest that GSN does not selectively target HIV-1 Env but likely increases the lysosomal turnover of multiple membrane proteins. Exactly how GSN accomplishes this task remains the subject of future investigations. Nevertheless, the Vpr-induced degradation of GSN, as implied by the results from Fig. 6, is likely to have pleiotropic effects, and this may further complicate our understanding of the precise role of Vpr in HIV-1 replication in macrophages.

## MATERIALS AND METHODS

**Affinity purification of Vpr-interacting THP-1 proteins and mass spectrometry.** To avoid the premature degradation of Vpr targets in THP-1 cells, we first purified the bait (i.e., Flag-tagged Vpr and, as a control, Flag-tagged GFP-N) from transiently transfected HEK293T cells, and we and immobilized it on Flag beads (EZview RedAnti-FLAG M2 affinity gel; Sigma-Aldrich [cat. number F2426]). The beads were washed 3 times with cold lysis buffer (50 mM Tris [pH 7.5], 150 mM NaCl, 10% glycerol, 1% Triton X-100) and were then exposed to cell extract from  $1.5 \times 10^8$  PMA-treated THP-1 cells. Samples were incubated for 20 h at 4°C on a rotator platform. The beads were then washed 3 times with cold lysis buffer, and bound proteins were eluted via the addition of 120  $\mu$ L of FLAG peptide (165  $\mu$ g/mL; Millipore Sigma; cat. number F4799) in lysis buffer. Mass spectrometry was performed at the Harvard University Mass Spectrometry and Proteomics Resource Laboratory (Cambridge, MA). Because we recovered more peptides from the Vpr pulldown (4,173) than the GFP-N pulldown (2,727), all of the downstream analyses were performed using a normalized Vpr:GFP-N peptide ratio: (number of peptides in Vpr pulldown) / (number of peptides in GFP-N pulldown)  $\cdot$  0.65. The constant is the ratio of total peptides in the GFP-N to Vpr pulldowns (2,727 / 4,173 = 0.65). The identities of the recovered proteins were determined by mapping the recovered peptide sequences to the human proteome.

**Cells.** HEK293T and TZM-bl cells were maintained in DMEM with 4.5 g/L glucose (Sigma-Aldrich, St. Louis, MO) that was supplemented with 10% fetal bovine serum, 100 U/mL penicillin, and 100 mg/mL streptomycin. THP-1 cells were grown in complete RPMI medium supplemented with 10% fetal bovine serum, 100 U/mL penicillin, and 100  $\mu$ g/mL streptomycin. The differentiation of THP-1 cells was achieved by growing cells for 48 h in the presence of PMA (100 ng/mL), and this was followed by a resting period of 24 h, as described (42). Elutriated human monocytes from multiple anonymous normal donors were obtained from the NIH blood bank under protocol 99-CC-0168: "Collection and Distribution of Blood Components from Healthy Donors for In Vitro Research Use". Monocytes ( $4 \times 10^6$  cells/well in a 6-well plate) were cultured in 2 mL of complete DMEM supplemented with 10% pooled human serum (Gemini Bio-Products, West Sacramento, CA) and 1 mM sodium pyruvate (Thermo Fisher Scientific, Atlanta, GA 30384) for 5 to 7 days to allow for differentiation into macrophages (MDMs).

**Plasmids and viral vectors.** The infectious molecular clones pNL4-3 (43) and pAD8 (44) have been reported previously. Vpr-defective variants were created by filling in an EcoRI site in the *vpr* gene, resulting in the translational frameshift and premature termination of the Vpr ORFs. The SIVcpz molecular clone pSIVcpzMB897 (45) was a gift from Beatrice Hahn and was used as the template for the construction of the SIVcpz Vpr expression vectors. For the expression of the N-terminally Flag-tagged Vpr proteins, *vpr* sequences from pNL4-3, pAD8, and SIVcpz were PCR amplified and cloned into p3xFlag-CMV-7.1 (Sigma-Aldrich, St. Louis, MO). The DCAF1 binding mutants of Vpr (Q65R) were created via site-directed PCR-based mutagenesis. As a nonspecific control, an N-terminally Flag-tagged GFP construct was created via the PCR amplification of the 5'-end of the *gfp* gene (corresponding to the N-terminal 95 amino acids of GFP) and cloning into p3xFlag-CMV-7.1. The resulting Flag-GFP-N construct expresses a protein that is of a similar size to those of the Flag-Vpr constructs. A GSN cDNA clone (NM\_002438) in the backbone of pOTB7 was purchased from Dharmacon (clone ID: 4661084). For expression in mammalian cells, the *gsn* gene was PCR amplified using primers for creating untagged or N-terminally Flag-tagged vectors in the backbone of pVR1012 (46).

**Production of a GSN-specific polyclonal antibody in rabbits.** A DNA fragment corresponding to the C-terminal 266 residues (residues 516 to 782) of GSN (GSN 40K) was PCR amplified and cloned into the *E. coli* expression vector pPLc24 (47) in-frame with the N-terminal portion (residues 1 to 99) of the bacteriophage MS2 polymerase. The encoded 365 residue MS2-GSN fusion protein had a predicted molecular mass of about 40 kDa (hence the designation GSN 40K). The detailed methodology for the expression of the MS2 fusion proteins, protein purification, and immunization of rabbits has been described previously (48). Briefly, the pPLc24-based expression system uses a thermolabile lambda repressor that is encoded on a separate kanamycin selectable vector and is inactivated by shifting cultures from 28°C to 42°C. The vector encoding the MS2-GSN fusion protein is selectable by ampicillin. The MS2-GSN encoding vector was transformed into bacteria containing the kanamycin selected lambda repressor plasmid. Cultures were grown in the presence of ampicillin (100  $\mu$ g/mL) and kanamycin (30  $\mu$ g/mL) to a high density (up to 48 h) at 28°C with slow shaking. For the induction of protein synthesis, cultures were diluted 1:5 in prewarmed (42°C) LB-broth without antibiotics and incubated with vigorous shaking at 42°C for 2.5 h. Induced recombinant proteins accumulated in inclusion bodies and were purified via the sequential extraction of the bacterial pellet with increasing concentrations of urea.

Typically, the fusion protein was solubilized at 8 M urea. The proteins were further purified via preparative gel electrophoresis. To extract the protein from the acrylamide gel, the gels were briefly stained with Coomassie blue to locate the MS2-GSN fusion protein. The corresponding region was cut from the gel and incubated in PBS/0.1% SDS at 65°C overnight (ON) to extract the fusion protein from the acrylamide. The Coomassie blue served as a tracer during the extraction process. The extracted protein was filtered through a 0.45  $\mu\text{m}$  filter to eliminate residual acrylamide and was then concentrated under a vacuum (Speed Vac centrifuge) to approximately 1 mg/mL. The protein was dialyzed ON at room temperature against PBS/0.1% SDS. Purified recombinant protein was used to immunize rabbits.

**Transient transfection of HEK293T cells.** For the transient transfection of HEK293T cells,  $3 \times 10^6$  cells were plated in a 25  $\text{cm}^2$  flask and grown overnight. The following day, the cells were transfected using Lipofectamine PLUS (Invitrogen, Carlsbad, CA), according to the manufacturer's instructions. Typically, the total amounts of plasmid DNAs in all samples were adjusted to 5 or 6  $\mu\text{g}$ , using empty vector DNA as appropriate. After 24 h, the cells were scraped, washed with PBS, suspended in PBS (100  $\mu\text{L}/10^6$  cells), and mixed with an equal volume of 2 $\times$  sample buffer (SB) (4% SDS, 125 mM Tris-HCl [pH 6.8], 10% 2-mercaptoethanol, 10% glycerol, 0.002% bromophenol blue). For the analysis of the virus-associated proteins, virus-containing culture supernatants were harvested and precleared via low-speed centrifugation (5 min, 1,500 rpm). Supernatants were then filtered through a 0.45  $\mu\text{m}$  syringe filter and concentrated via pelleting in a refrigerated minicentrifuge (90 min, 14,000 rpm, 4°C). The pellets were lysed in a 60  $\mu\text{L}/1.3$  mL input of 2 $\times$  SB and processed for immunoblot analysis.

**Virus replication in MDMs.** The virus stocks for the infection of MDMs were prepared as follows. HEK293T cells (in 75  $\text{cm}^2$  flasks) were transfected with 15  $\mu\text{g}$  of proviral DNA using Lipofectamine PLUS (Invitrogen, Carlsbad, CA), according to the manufacturer's instructions. To produce VSV-G-pseudotyped virus stocks, 1.5  $\mu\text{g}$  of pCMV-VSV-G vector DNA was cotransfected with 13.5  $\mu\text{g}$  of pAD8 DNA. Virus-containing supernatants were harvested 2 days later, and cellular debris were removed via centrifugation (5 min, 1,500 rpm). This was followed by filtration (0.45  $\mu\text{m}$ ). The virus was concentrated via ultracentrifugation (75 min, 35,000 rpm, 4°C) and suspended in 1.5 mL of DMEM. For the infection of the MDMs, the culture medium was removed from the cells and replaced with 0.5 mL of virus stock. The virus was allowed to adsorb for 3 h at 37°C before the medium was replaced by 2 mL of complete DMEM supplemented with 10% human serum. Half of the medium (1 mL) was replaced with fresh medium every 2 to 3 days. For the immunoblot analysis, the MDMs were washed once with PBS, suspended in PBS, mixed with an equal volume of 2 $\times$  SB, and heated at 95°C for 5 to 10 min.

**Immunoblot analysis.** For the immunoblot analysis of the intracellular proteins, the cells were washed once with PBS, suspended in PBS (100  $\mu\text{L}/10^6$  cells), and mixed with an equal volume of 2 $\times$  SB. For the immunoblot analysis of the virus-associated proteins, virus-containing supernatants were pelleted in a refrigerated Eppendorf minicentrifuge at 14,000 rpm for 90 min (4°C). The pelleted viral proteins were solubilized via the addition of a 60  $\mu\text{L}$  SB/1.3 mL sample. The samples were heated at 95°C with occasional vortexing until they were completely dissolved. The samples were subjected to SDS-PAGE, transferred to polyvinylidene difluoride (PVDF) membranes, and reacted with primary antibodies, as described in the text. GSN was identified using an antibody to GSN that was raised in rabbits against the recombinant protein-encompassing residues 518 to 782 of human GSN. In experiments in which epitope-tagged proteins were used, tag-specific antibodies were employed as primary antibodies. HIV-1 Gag was identified using pooled HIV immunoglobulin (HIV-Ig; NIH Research and Reference Reagent Program; cat. number 3957), and tubulin was identified using a mouse monoclonal antibody to  $\alpha$ -tubulin (T9026; Sigma-Aldrich, St. Louis, MO). HIV-1 Env was detected using a rabbit polyclonal antibody to recombinant gp120. The membranes were then incubated with horseradish peroxidase-conjugated secondary antibodies (GE Healthcare, Piscataway, NJ), and the proteins were visualized via enhanced chemiluminescence (Clarity Western ECL substrate 170 to 5,061; Bio-Rad Laboratories, Hercules, CA), using Bio-Rad Image Lab for the data acquisition and image processing.

**Metabolic labeling and pulse-chase analysis.** For the pulse-chase analysis, HEK293T cells were grown as described before. For the transient transfection,  $3 \times 10^6$  cells were plated in a 25  $\text{cm}^2$  flask and grown overnight. The following day, the cells were transfected using Lipofectamine Plus (Invitrogen), according to the manufacturer's instructions. The total amounts of plasmid DNA in all samples were equalized with empty vector DNA as appropriate. After 24 h, the transfected HEK293T cells were harvested via scraping, washed with PBS, and suspended in 7 mL of labeling medium (methionine- and cysteine-free RPMI [MP Biomedical, Solon, OH] containing 5% fetal calf serum [FCS]). The samples were incubated for 20 min in either the presence of MG132 (10  $\mu\text{M}$ ) or the equivalent volume of DMSO at 37°C to deplete the intracellular methionine/cysteine pool. The cells were then labeled for 15 min at 37°C in 200  $\mu\text{L}$  of labeling medium supplemented with 30  $\mu\text{L}$  (300  $\mu\text{Ci}$ ) of [ $^{35}\text{S}$ ]-Expres $^{35}\text{S}$ -label (NEG072; PerkinElmer). After the labeling period, unincorporated isotope was removed, and equal aliquots of cells were added to 1 mL of prewarmed complete DMEM and chased for the selected times. Cells and virus-containing supernatants were harvested separately at each time point and were stored on dry ice until all samples had been collected. For the immunoprecipitation, the cells were lysed in 1 mL of Triton X-100-based lysis buffer (50 mM Tris-HCl [pH 7.5], 150 mM NaCl, 1% Triton X-100, 10% glycerol) and incubated at 4°C on a rotating platform for 20 min. After lysis, insoluble material was pelleted at 10,000 rpm for 10 min, and the clarified supernatants were added to protein A-Sepharose beads (Sigma-Aldrich, St. Louis, MO; cat. number P3391) that had been preadsorbed with anti-GSN polyclonal antibodies (5  $\mu\text{L}$  plasma/IP in 1 mL lysis buffer). The samples were adjusted to a 1.3 mL total volume with lysis buffer and were incubated for 1 h at 4°C on a rotating platform. The beads were then washed three times with 1 mL each of lysis buffer. The precipitated proteins were solubilized via boiling in 100  $\mu\text{L}$  SB, and they were separated via SDS-PAGE. The gels were fixed and dried. The gels were exposed

**TABLE 1** DNA oligonucleotides used for semiquantitative RT-PCR

Oligonucleotide	Sequence
HIV-1	
#1544 (exon 1)	5'-CTTGAAAGCGAAAGTAAAGC-3'
#3632 (exon 4)	5'-TGGATGCTCCAGGGCTC-3'
#3392 (exon 7)	5'-CGTCCCAGATAAGTGCTAAGG-3'
#640 (intron 4)	5'-CAATACTACTTCTGTGGTTGG-3'
hGH	
#1224	5'-TCTCCAGCCTCCCATCAGCGTTTGG-3'
#1225	5'-CAACAGAAATCCAACCTAGAGCTGCT-3'

to Kodak XMR film, and the proteins were visualized via fluorography. For protein quantitation, the gels were exposed to imaging plates. The plates were read using a Typhoon FLA 9500 Phosphorimager, and the quantitation of the data was done using FujiFilm Multi Gauge software.

**Quantitation of protein bands.** All of the immunoblot data were collected using a Bio-Rad ChemiDoc Imaging system. For the quantitation of Env proteins (Fig. 6A and B, 7, and 11) and GSN (Fig. 12), high-resolution Tagged Image File Format (TIFF) images that were created by the Bio-Rad ChemiDoc system were imported into the FujiFilm Multi Gauge software package. Bands corresponding to gp160/gp120, as well as CA, in the corresponding lanes were quantified and exported into an Excel spreadsheet. Note that for consistency, both gp160 and gp120 were quantified, and their combined values were used as the Env signal in the analysis. To be able to combine the results from multiple experiments into one figure, values obtained in the absence of GSN or Vpr were defined as 100%, and the remaining samples were expressed as fractions of the controls.

**Viral infectivity assay.** Virus-containing supernatants were precleared via low-speed centrifugation (5 min, 1,500 rpm) and filtered through a 0.45  $\mu$ m syringe filter. TZM-bl indicator cells (CD4<sup>+</sup>, CCR5<sup>+</sup>, CXCR4<sup>+</sup>) were plated in a 24-well plate (1 mL;  $5 \times 10^4$  cells/well) and infected in triplicate with 150  $\mu$ L each of viral supernatant. 48 h later, the cells were lysed in the wells with 250  $\mu$ L of 1 $\times$  Promega reporter lysis buffer (Promega; cat. number E1910). The luciferase activity in the lysate was determined by combining 15  $\mu$ L of each lysate with 50  $\mu$ L of luciferase substrate (Steady-Glo; Promega, Madison, WI). The light emission was measured using a GloMax microplate reader (Promega). The values were normalized for equal reverse transcriptase activity.

**OptiPrep density gradient centrifugation.** The culture supernatants (11 mL) were pelleted in an SW41 rotor (Beckman) for 75 min at 35,000 rpm and 4°C. The pellets were suspended in 500  $\mu$ L RPMI (without FBS) and subjected to OptiPrep density gradient centrifugation, essentially as described (49). Specifically, 9 OptiPrep dilutions (30% to 6% in 3% increments) were prepared by diluting the 60% (wt/vol) stock solution (Sigma-Aldrich, St. Louis, MO; cat. number D1556) in PBS. Starting with the 30% solution, 445  $\mu$ L of each dilution were sequentially added to a SW55 tube (total volume = 4,005  $\mu$ L). The gradient was then overlaid with 500  $\mu$ L of the concentrated culture supernatants and subjected to ultracentrifugation (Beckman SW55Ti rotor; 45,000 rpm, 90 min at 4°C). 12 fractions (380  $\mu$ L each) were then collected from the tops of the gradients and mixed with 150  $\mu$ L each of 4 $\times$  SB (8% SDS, 250 mM Tris [pH 6.8], 20% 2-mercaptoethanol, 20% glycerol, 0.005% bromophenol blue). The samples were heated to 95°C for 10 min with occasional vortexing. The samples (90  $\mu$ L each) were then run on SDS-PAGE and processed for immunoblot analysis.

**Effect of GSN on the viral mRNA splicing pattern.** For RNA and protein isolation,  $2.5 \times 10^5$  HEK293T cells were transfected with 1  $\mu$ g each of pNL4-3, pVR-GSN, pVR-Flag GSN, and pXGH5 using the TransIT-LT1 transfection reagent (Mirus Bio LLC), according to the manufacturer's instructions. 24 h after transfection, the cells were harvested and washed with PBS. Total RNA was isolated using acid guanidinium thiocyanate-phenol-chloroform. The splicing patterns were analyzed via semiquantitative RT-PCR. For reverse transcription, 2  $\mu$ g of total RNA were subjected to cDNA synthesis. cDNA synthesis was performed for 1 h at 50°C and for 15 min at 72°C by using 200 U Superscript III RNase H Reverse Transcriptase (Invitrogen), 7.5 pmol oligonucleotide(dT)12-18 (Roche) as a primer, 20 U of RNAsin (Promega, Fitchburg, WI), and 10 mM of deoxynucleoside triphosphate (Qiagen, Hilden, Germany). The cDNA was used as a template for the semiquantitative PCRs, using the following primer pairs (Table 1): #1544/#3392 (2 kb species), #1544/#640 (4 kb species), #1544/#3632 (Ex1-4 splicing), and #1224/#1225 (hGH). The PCR products were separated on 10% nondenaturing polyacrylamide gels, stained with ethidium bromide, and visualized with an Imager (INTAS Science Imaging, Göttingen, Germany).

**Statistical analysis.** The average values of all of the data are presented, with error bars indicating the standard error of the mean. Statistical significance was analyzed in GraphPad Prism (v9.4.1), using an ordinary one-way ANOVA and a *post hoc* Tukey's, Sidak's or Dunnett's test, as appropriate. *P* values are depicted as \*, *P* < 0.05; \*\*, *P* < 0.01; \*\*\*, *P* < 0.001.

## SUPPLEMENTAL MATERIAL

Supplemental material is available online only.

**FIG S1**, JPG file, 2.6 MB.

**FIG S2**, JPG file, 0.8 MB.



## ACKNOWLEDGMENTS

We thank Chunling Gao and Kathleen Clouse for their help with the elutriation of the monocytes. The following reagents were obtained through the NIH HIV Reagent Program, Division of AIDS, NIAID, NIH: HIV-1 immunoglobulin (cat. number 3957), contributed by the NABI and the National Heart Lung and Blood Institute (Luiz Barbosa). This work was supported by the Intramural Research Program of the NIH, NIAID (1 Z01 AI000669; K.S.).

H.F., S.S., and K.S. designed the study. H.F., S.S., E.M., L.T., S.K., D.F., H.S., F.H., and K.S. performed the experiments. H.F. and K.S. wrote the manuscript.

We declare no competing interests.

## REFERENCES

- Schrofelbauer B, Hakata Y, Landau NR. 2007. HIV-1 Vpr function is mediated by interaction with the damage-specific DNA-binding protein DDB1. *Proc Natl Acad Sci U S A* 104:4130–4135. <https://doi.org/10.1073/pnas.0610167104>.
- Okumura A, Alce T, Lubyova B, Ezelle H, Strebek K, Pitha PM. 2008. HIV-1 accessory proteins VPR and Vif modulate antiviral response by targeting IRF-3 for degradation. *Virology* 373:85–97. <https://doi.org/10.1016/j.virol.2007.10.042>.
- Maudet C, Sourisce A, Dragin L, Lahouassa H, Rain JC, Bouaziz S, Ramirez BC, Margottin-Goguet F. 2013. HIV-1 Vpr induces the degradation of ZIP and sZIP, adaptors of the NuRD chromatin remodeling complex, by hijacking DCAF1/VprBP. *PLoS One* 8:e77320. <https://doi.org/10.1371/journal.pone.0077320>.
- Romani B, Shaykh Baygloo N, Aghasadeghi MR, Allahbakhshi E. 2015. HIV-1 Vpr protein enhances proteasomal degradation of MCM10 DNA replication factor through the Cul4-DDB1[VprBP] E3 ubiquitin ligase to induce G2/M cell cycle arrest. *J Biol Chem* 290:17380–17389. <https://doi.org/10.1074/jbc.M115.641522>.
- Romani B, Baygloo NS, Hamidi-Fard M, Aghasadeghi MR, Allahbakhshi E. 2016. HIV-1 Vpr protein induces proteasomal degradation of chromatin-associated class I HDACs to overcome latent infection of macrophages. *J Biol Chem* 291:2696–2711. <https://doi.org/10.1074/jbc.M115.689018>.
- Forouzanfar F, Ali S, Wallet C, De Rovere M, Ducloy C, El Mekdad H, El Maassarani M, Ait-Ammar A, Van Assche J, Boutant E, Daouad F, Margottin-Goguet F, Moog C, Van Lint C, Schwartz C, Rohr O. 2019. HIV-1 Vpr mediates the depletion of the cellular repressor CTIP2 to counteract viral gene silencing. *Sci Rep* 9:13154. <https://doi.org/10.1038/s41598-019-48689-x>.
- Lahouassa H, Blondot ML, Chauveau L, Chougui G, Morel M, Leduc M, Guillonnet F, Ramirez BC, Schwartz O, Margottin-Goguet F. 2016. HIV-1 Vpr degrades the HLTf DNA translocase in T cells and macrophages. *Proc Natl Acad Sci U S A* 113:5311–5316. <https://doi.org/10.1073/pnas.1600485113>.
- Zhou X, DeLucia M, Hao C, Hrecka K, Monnie C, Skowronski J, Ahn J. 2017. HIV-1 Vpr protein directly loads helicase-like transcription factor (HLTF) onto the CRL4-DCAF1 E3 ubiquitin ligase. *J Biol Chem* 292:21117–21127. <https://doi.org/10.1074/jbc.M117.798801>.
- Yan J, Shun MC, Zhang Y, Hao C, Skowronski J. 2019. HIV-1 Vpr counteracts HLTf-mediated restriction of HIV-1 infection in T cells. *Proc Natl Acad Sci U S A* 116:9568–9577. <https://doi.org/10.1073/pnas.1818401116>.
- Yan J, Shun MC, Hao C, Zhang Y, Qian J, Hrecka K, DeLucia M, Monnie C, Ahn J, Skowronski J. 2018. HIV-1 Vpr reprograms CLR4(DCAF1) E3 ubiquitin ligase to antagonize exonuclease 1-mediated restriction of HIV-1 infection. *mBio* 9:e01732-18. <https://doi.org/10.1128/mBio.01732-18>.
- Zhang Q, Kang Y, Wang S, Gonzalez GM, Li W, Hui H, Wang Y, Rana TM. 2021. HIV reprograms host m(6)Am RNA methylome by viral Vpr protein-mediated degradation of PCIF1. *Nat Commun* 12:5543. <https://doi.org/10.1038/s41467-021-25683-4>.
- Le Rouzic E, Belaidouni N, Estrabaud E, Morel M, Rain JC, Transy C, Margottin-Goguet F. 2007. HIV1 Vpr arrests the cell cycle by recruiting DCAF1/VprBP, a receptor of the Cul4-DDB1 ubiquitin ligase. *Cell Cycle* 6:182–188. <https://doi.org/10.4161/cc.6.2.3732>.
- Wen X, Duus KM, Friedrich TD, de Noronha CM. 2007. The HIV1 protein Vpr acts to promote G2 cell cycle arrest by engaging a DDB1 and Cullin4A-containing ubiquitin ligase complex using VprBP/DCAF1 as an adaptor. *J Biol Chem* 282:27046–27057. <https://doi.org/10.1074/jbc.M70395200>.
- Ahn J, Vu T, Novince Z, Guerrero-Santoro J, Rapic-Otrin V, Gronenborn AM. 2010. HIV-1 Vpr loads uracil DNA glycosylase-2 onto DCAF1, a substrate recognition subunit of a cullin 4A-ring E3 ubiquitin ligase for proteasome-dependent degradation. *J Biol Chem* 285:37333–37341. <https://doi.org/10.1074/jbc.M110.133181>.
- Mazur AJ, Morosan-Puopolo G, Makowiecka A, Malicka-Błaskiewicz M, Nowak D, Brand-Saberi B. 2016. Analysis of gelsolin expression pattern in developing chicken embryo reveals high GSN expression level in tissues of neural crest origin. *Brain Struct Funct* 221:515–534. <https://doi.org/10.1007/s00429-014-0923-5>.
- Kwiatkowski DJ, Stosel TP, Orkin SH, Mole JE, Colten HR, Yin HL. 1986. Plasma and cytoplasmic gelsolins are encoded by a single gene and contain a duplicated actin-binding domain. *Nature* 323:455–458. <https://doi.org/10.1038/323455a0>.
- Jagadish T, Pottiez G, Fox HS, Ciborowski P. 2012. Plasma gelsolin accumulates in macrophage nodules in brains of simian immunodeficiency virus infected rhesus macaques. *J Neurovirol* 18:113–119. <https://doi.org/10.1007/s13365-012-0085-2>.
- Pottiez G, Haverland N, Ciborowski P. 2010. Mass spectrometric characterization of gelsolin isoforms. *Rapid Commun Mass Spectrom* 24:2620–2624. <https://doi.org/10.1002/rcm.4681>.
- Nag S, Larsson M, Robinson RC, Burtinck LD. 2013. Gelsolin: the tail of a molecular gymnast. *Cytoskeleton (Hoboken)* 70:360–384. <https://doi.org/10.1002/cm.21117>.
- Li GH, Arora PD, Chen Y, McCulloch CA, Liu P. 2012. Multifunctional roles of gelsolin in health and diseases. *Med Res Rev* 32:999–1025. <https://doi.org/10.1002/med.20231>.
- Asch HL, Head K, Dong Y, Natoli F, Winston JS, Connolly JL, Asch BB. 1996. Widespread loss of gelsolin in breast cancers of humans, mice, and rats. *Cancer Res* 56:4841–4845.
- Mullauer L, Fujita H, Ishizaki A, Kuzumaki N. 1993. Tumor-suppressive function of mutated gelsolin in ras-transformed cells. *Oncogene* 8:2531–2536.
- Vandekerckhove J, Bauw G, Vancompernelle K, Honore B, Celis J. 1990. Comparative two-dimensional gel analysis and microsequencing identifies gelsolin as one of the most prominent downregulated markers of transformed human fibroblast and epithelial cells. *J Cell Biol* 111:95–102. <https://doi.org/10.1083/jcb.111.1.95>.
- Tanaka M, Mullauer L, Ogiso Y, Fujita H, Moriya S, Furuuchi K, Harabayashi T, Shinohara N, Koyanagi T, Kuzumaki N. 1995. Gelsolin: a candidate for suppressor of human bladder cancer. *Cancer Res* 55:3228–3232.
- Fettucciari K, Ponsini P, Palumbo C, Rosati E, Mannucci R, Bianchini R, Modesti A, Marconi P. 2015. Macrophage induced gelsolin in response to Group B Streptococcus (GBS) infection. *Cell Microbiol* 17:79–104. <https://doi.org/10.1111/cmi.12338>.
- Cheng Y, Hu X, Liu C, Chen M, Wang J, Wang M, Gao F, Han J, Zhang C, Sun D, Min R. 2017. Gelsolin inhibits the inflammatory process induced by LPS. *Cell Physiol Biochem* 41:205–212. <https://doi.org/10.1159/000456043>.
- Qiao H, McMillan JR. 2007. Gelsolin segment 5 inhibits HIV-induced T-cell apoptosis via Vpr-binding to VDAC. *FEBS Lett* 581:535–540. <https://doi.org/10.1016/j.febslet.2006.12.057>.
- Garcia-Exposito L, Ziglio S, Barroso-Gonzalez J, de Armas-Rillo L, Valera MS, Zipeto D, Machado JD, Valenzuela-Fernandez A. 2013. Gelsolin activity controls efficient early HIV-1 infection. *Retrovirology* 10:39. <https://doi.org/10.1186/1742-4690-10-39>.
- Fabryova H, Strebek K. 2019. Vpr and its cellular interaction partners: R where yet? *Cells* 8:1310. <https://doi.org/10.3390/cells811310>.

30. Cooper JA, Schafer DA. 2000. Control of actin assembly and disassembly at filament ends. *Curr Opin Cell Biol* 12:97–103. [https://doi.org/10.1016/S0955-0674\(99\)00062-9](https://doi.org/10.1016/S0955-0674(99)00062-9).
31. Sun HQ, Yamamoto M, Mejillano M, Yin HL. 1999. Gelsolin, a multifunctional actin regulatory protein. *J Biol Chem* 274:33179–33182. <https://doi.org/10.1074/jbc.274.47.33179>.
32. Argyris EG, Acheampong E, Wang F, Huang J, Chen K, Mukhtar M, Zhang H. 2007. The interferon-induced expression of APOBEC3G in human blood-brain barrier exerts a potent intrinsic immunity to block HIV-1 entry to central nervous system. *Virology* 367:440–451. <https://doi.org/10.1016/j.virol.2007.06.010>.
33. Stenglein MD, Burns MB, Li M, Lengyel J, Harris RS. 2010. APOBEC3 proteins mediate the clearance of foreign DNA from human cells. *Nat Struct Mol Biol* 17:222–229. <https://doi.org/10.1038/nsmb.1744>.
34. DeHart JL, Zimmerman ES, Ardon O, Monteiro-Filho CM, Arganaraz ER, Planelles V. 2007. HIV-1 Vpr activates the G2 checkpoint through manipulation of the ubiquitin proteasome system. *Virology* 363:261–271. <https://doi.org/10.1016/j.virol.2007.01.022>.
35. Wiederin J, Rozek W, Duan F, Ciborowski P. 2009. Biomarkers of HIV-1 associated dementia: proteomic investigation of sera. *Proteome Sci* 7:8. <https://doi.org/10.1186/1477-5956-7-8>.
36. Schubert U, Bour S, Willey RL, Strebel K. 1999. Regulation of virus release by the macrophage-tropic human immunodeficiency virus type 1 AD8 isolate is redundant and can be controlled by either Vpr or Env. *J Virol* 73:887–896. <https://doi.org/10.1128/JVI.73.2.887-896.1999>.
37. Krummheuer J, Johnson AT, Hauber I, Kammler S, Anderson JL, Hauber J, Purcell DF, Schaal H. 2007. A minimal uORF within the HIV-1 vpr leader allows efficient translation initiation at the downstream env AUG. *Virology* 363:261–271. <https://doi.org/10.1016/j.virol.2007.01.022>.
38. Piktel E, Levental I, Durnas B, Janmey PA, Bucki R. 2018. Plasma gelsolin: indicator of inflammation and its potential as a diagnostic tool and therapeutic target. *Int J Mol Sci* 19. <https://doi.org/10.3390/ijms19092516>.
39. Mashiba M, Collins DR, Terry VH, Collins KL. 2014. Vpr overcomes macrophage-specific restriction of HIV-1 Env expression and virion production. *Cell Host Microbe* 16:722–735. <https://doi.org/10.1016/j.chom.2014.10.014>.
40. Zhang X, Zhou T, Frabutt DA, Zheng YH. 2016. HIV-1 Vpr increases Env expression by preventing Env from endoplasmic reticulum-associated protein degradation (ERAD). *Virology* 496:194–202. <https://doi.org/10.1016/j.virol.2016.06.002>.
41. Lubow J, Virgilio MC, Merlino M, Collins DR, Mashiba M, Peterson BG, Lukic Z, Painter MM, Gomez-Rivera F, Terry V, Zimmerman G, Collins KL. 2020. Mannose receptor is an HIV restriction factor counteracted by Vpr in macrophages. *Elife* 9. <https://doi.org/10.7554/eLife.51035>.
42. Chanput W, Mes JJ, Wichers HJ. 2014. THP-1 cell line: an in vitro cell model for immune modulation approach. *Int Immunopharmacol* 23:37–45. <https://doi.org/10.1016/j.intimp.2014.08.002>.
43. Adachi A, Gendelman HE, Koenig S, Folks T, Willey R, Rabson A, Martin MA. 1986. Production of acquired immunodeficiency syndrome-associated retrovirus in human and nonhuman cells transfected with an infectious molecular clone. *J Virol* 59:284–291. <https://doi.org/10.1128/JVI.59.2.284-291.1986>.
44. Theodore TS, Englund G, Buckler-White A, Buckler CE, Martin MA, Peden KW. 1996. Construction and characterization of a stable full-length macrophage-tropic HIV type 1 molecular clone that directs the production of high titers of progeny virions. *AIDS Res Hum Retroviruses* 12:191–194. <https://doi.org/10.1089/aid.1996.12.191>.
45. Van Heuverswyn F, Li Y, Bailes E, Neel C, Lafay B, Keele BF, Shaw KS, Takehisa J, Kraus MH, Loul S, Butel C, Liegeois F, Yangda B, Sharp PM, Mpoudi-Ngole E, Delaporte E, Hahn BH, Peeters M. 2007. Genetic diversity and phylogeographic clustering of SIVcpzPtt in wild chimpanzees in Cameroon. *Virology* 368:155–171. <https://doi.org/10.1016/j.virol.2007.06.018>.
46. Yu X, Yu Y, Liu B, Luo K, Kong W, Mao P, Yu XF. 2003. Induction of APOBEC3G ubiquitination and degradation by an HIV-1 Vif-Cul5-SCF complex. *Science* 302:1056–1060. <https://doi.org/10.1126/science.1089591>.
47. Remaut E, Stanssens P, Fiers W. 1981. Plasmid vectors for high-efficiency expression controlled by the PL promoter of coliphage lambda. *Gene* 15:81–93. [https://doi.org/10.1016/0378-1119\(81\)90106-2](https://doi.org/10.1016/0378-1119(81)90106-2).
48. Strebel K, Beck E, Strohmaier K, Schaller H. 1986. Characterization of foot and mouth disease virus gene products with antisera against bacterially synthesized fusion proteins. *J Virol* 57:983–991. <https://doi.org/10.1128/JVI.57.3.983-991.1986>.
49. Dettenhofer M, Yu XF. 1999. Highly purified human immunodeficiency virus type 1 reveals a virtual absence of Vif in virions. *J Virol* 73:1460–1467. <https://doi.org/10.1128/JVI.73.2.1460-1467.1999>.
50. Willey RL, Smith DH, Lasky LA, Theodore TS, Earl PL, Moss B, Capon DJ, Martin MA. 1988. In vitro mutagenesis identifies a region within the envelope gene of the human immunodeficiency virus that is critical for infectivity. *J Virol* 62:139–147. <https://doi.org/10.1128/JVI.62.1.139-147.1988>.
51. Zhang W, Du J, Evans SL, Yu Y, Yu XF. 2011. T-cell differentiation factor CBF-beta regulates HIV-1 Vif-mediated evasion of host restriction. *Nature* 481:376–379. <https://doi.org/10.1038/nature10718>.
52. Purcell DFJ, Martin MA. 1993. Alternative splicing of human immunodeficiency virus type 1 mRNA modulates viral protein expression, replication, and infectivity. *J Virol* 67:6365–6378. <https://doi.org/10.1128/JVI.67.11.6365-6378.1993>.